1   **Comparison of model and ground observations finds snowpack and blowing snow aerosols both**

2   **contribute to Arctic tropospheric reactive bromine**

3   William F. Swanson[1], Chris D. Holmes[2], William R. Simpson[1], Kaitlyn Confer[3], Louis Marelle[45], Jennie

4   L. Thomas[4], Lyatt Jaeglé[3], Becky Alexander[3], Shuting Zhai[3], Qianjie Chen[6], Xuan Wang[7], Tomás

5   Sherwen[89]

6   [1]Department of Chemistry and Biochemistry and Geophysical Institute, University of Alaska Fairbanks,

7   Fairbanks, Alaska

8   [2]Department of Earth, Ocean and Atmospheric Science, Florida State University, Tallahassee, Florida

9   [3]Department of Atmospheric Sciences, University of Washington, Seattle, Washington

10   [4]Institut des Géosciences de l'Environnement (IGE), Institut Polytechnique de Grenoble, Grenoble, France

11   [5]Laboratoire Atmosphères Observations Spatiales (LATMOS), Sorbonne Université, Paris, France

12   [6]Department of Civil and Environmental Engineering, Hong Kong Polytechnic University, Hong Kong,

13   China

14   [7]School of Energy and the Environment, City University of Hong Kong, Hong Kong, China

15   [8]National Centre for Atmospheric Science, University of York, York, UK.

16   [9]Department of Chemistry, University of York, York, United Kingdom

17   *Correspondence to:* William F. Swanson (wswanson3@alaska.edu)

18   **Abstract**

19   Reactive halogens play a prominent role in the atmospheric chemistry of the Arctic during

20   springtime. Field measurements and modeling studies suggest that halogens are emitted to the atmosphere

21   from snowpack and reactions on wind-blown snow-sourced aerosols. The relative importance of

22   snowpack and blowing snow sources is still debated, both at local scales and regionally throughout the

23   Arctic. To understand implications of these halogen sources on a pan-Arctic scale, we simulate Arctic

24   reactive bromine chemistry in the atmospheric chemical transport model GEOS-Chem. Two mechanisms

25   are included: 1) a blowing snow sea salt aerosol formation mechanism and 2) a snowpack mechanism

26   assuming uniform molecular bromine production from all snow surfaces. We compare simulations

27   including neither mechanism, each mechanism individually, and both mechanisms to examine conditions

28   where one process may dominate or the mechanisms may interact. We compare the models using these

29   mechanisms to observations of bromine monoxide (BrO) derived from multiple-axis differential optical

30   absorption spectroscopy (MAX-DOAS) instruments on O-Buoy platforms on the sea ice and at a coastal

31   site in Utqiaġvik, Alaska during spring 2015. Model estimations of hourly and monthly average BrO are

32   improved by assuming a constant yield of 0.1% molecular bromine from all snowpack surfaces on ozone

33   deposition. The blowing snow aerosol mechanism increases modeled BrO by providing more bromide-

34 rich aerosol surface area for reactive bromine recycling. The snowpack mechanism led to increased model

35 BrO across the Arctic Ocean with maximum production in coastal regions, whereas the blowing snow

36 aerosol mechanism increases BrO in specific areas due to high surface wind speeds. Our uniform

37 snowpack source has a greater impact on BrO mixing ratios than the blowing snow source. Model results

38 best replicate several features of BrO observations during spring 2015 when using both mechanisms in

39 conjunction, adding evidence that these mechanisms are both active during the Arctic Spring. Extending

40 our transport model throughout the entire year leads to predictions of enhanced fall BrO that are not

41 supported by observations.

1. Introduction

43   Simulating Arctic halogen chemistry is a persistent problem for global models because processes

44 appear to differ between the Arctic and middle latitudes (Parrella et al., 2012; Schmidt et al., 2016).

45 Space-based instruments observe large column densities of reactive bromine across swaths of the Arctic

46 Ocean during the Arctic spring (Chance, 1998; Richter et al., 1998; Wagner and Platt, 1998). Increased

47 levels of tropospheric reactive bromine are associated with ozone depletion events (Barrie et al., 1988;

48 Foster et al., 2001; Koo et al., 2012; Halfacre et al., 2014) as well as oxidation of gaseous elemental

49 mercury (Schroeder et al., 1998; Nghiem, 2013; Moore et al., 2014). Bromine radicals have been

50 observed to lead directly to ozone depletion and mercury oxidation (Wang et al., 2019a). Deposition of

51 oxidized mercury to the snowpack can have deleterious effects on the health of Arctic humans and

52 animals (AMAP, 2011). Arctic reactive bromine chemistry impacts tropospheric oxidative chemistry but

53 is not typically accounted for in global models. Model studies have found that reactive halogen chemistry

54 can explain the oxidation of gaseous elemental mercury (Holmes et al., 2010) and reduce radiative forcing

55 from ozone (Sherwen et al., 2016c). Replicating reactive halogen chemistry in models requires inclusion

56 of multi-phase chemical reactions as well as mechanisms affecting sea salt aerosol particle production and

57 chemical reactions within the snowpack.

58   These increased levels of tropospheric reactive bromine radicals are a product of heterogeneous

59 photochemical reactions at the interface between air and saline surfaces such as surface snowpack and sea

60 salt aerosols (Saiz-Lopez and von Glasow, 2012; Simpson et al., 2015). Figure 1 depicts the gas-phase,

61 heterogeneous, and photochemical reactions thought to control tropospheric bromine, all of which are

62 included in the model and results presented in this manuscript. Bromine radicals (Br) are produced by

63 photolysis of molecular bromine (P1) or by self-reaction of BrO (R6) and react with ozone to form

64 bromine monoxide (BrO) (R2). Under sunlit conditions, BrO is most often photolyzed back to Br

65 radicals and an oxygen atom (P2) that then most often reforms ozone, resulting in a null cycle. Due to this

66 rapid interchange of Br and BrO, these two compounds form the BrO_x family. If processes other than BrO

67   photolysis (P2) convert BrO back to Br without producing ozone, the imbalance between these other

68   processes and P2 result in net ozone depletion. For example, ozone is depleted through R6 or R7 when

69   BrO reacts with another halogen oxide to form either Br_2 or BrCl, or through other more extended

70   processes. A reactive halogen activating cycle occurs when a BrO radical reacts with a hydroperoxy

71   (HO_2) radical in R5 to form gaseous hypobromous acid (HOBr). Heterogeneous chemistry can occur on a

72   saline surface between HOBr and particulate bromide (p-Br^-) in HR1 forming Br_2 or particle chloride (p-

73   Cl^-) in HR6 forming BrCl. For each cycle of reactions P1, R2, R5, and HR1, one hydroperoxy radical is

74   removed from the atmosphere, one bromine atom is released to the atmosphere, and one ozone molecule

75   is destroyed. This process of activation of particulate and snow bromide to Br_2 by consuming other

76   radicals (e.g. HO_2) is known as the "bromine explosion" (Wennberg, 1999). Ground-based instruments

77   have observed sharp increases in reactive bromine levels over the course of a single day from below 2

78   pmol/mol up to a maximum of 41 pmol/mol (Pöhler et al., 2010). Reactions may also sequester reactive

79   bromine into more stable bromine reservoir species. BrO may react with nitrogen dioxide (NO_2) in R8 to

80   form bromine nitrate ($BrNO_3$), which can also undergo hydrolysis on aqueous and ice surfaces to form

81   HOBr as in HR3.

Figure 1: GEOS-Chem tropospheric bromine reactions. Tropospheric bromide reservoirs shown in black boxes, with attached lines indicating reactions. Solid black lines R1-R11 indicate gas phase chemical reactions, solid orange lines P1-P8 indicate photolysis reactions, and dashed black lines HR1-HR8 indicate heterogeneous reactions. All gaseous species may undergo dry deposition. Additional sources of tropospheric bromine include the production of particulate bromide by the BLOW mechanisms and the production of Br_2 by the PACK mechanism, as well as the degradation of organobromines to form Br (OR1). Table 3 enumerates the specific species involved in each equation and shows reaction rates for each respective equation.

A potentially important competitor for recycling of reactive bromine through HOBr is its reaction with sulfur (IV) species, such as the reaction between HSO_3^- and HOBr in HR2 (Chen et al., 2017). To the extent that this reaction competes with HR1, it can slow the release of bromide from surfaces and reduce gas-phase reactive bromine (e.g., reduce BrO). Deposition of the HBr formed from HOBr by HR2 can remove reactive bromine from the troposphere. In general, the termination of this chemistry leads to formation of HBr, which undergoes gas-particulate uptake to particulate bromide (p-Br$^-$).

97   Ozone deposited to a saline surface can oxidize Br^- to form HOBr (similar to p-Br^- reactions

98   HR4a and HR4b) which is then converted to Br_2 or another dihalogen (e.g., BrCl). Production of reactive

99   bromine during ozone deposition does not require light and can occur at night (Oum et al., 1998; Artiglia

100   et al., 2017). The production of Br_2 is increased at low pH levels (Halfacre et al., 2019).

101   We define the inorganic bromine family, Br_y, in this manuscript as the sum of the bromine

102   species: Br, BrO, HOBr, $BrNO_3$, $2xBr_2$, BrCl, BrI, and HBr, excluding p-Br^-. The release of bromine from

103   sea salt aerosol particles was found to be the dominant global source of reactive bromine (Sander et al.,

104   2003; Zhu et al., 2019). Sea salt aerosol particles (SSA) are one of the most abundant aerosol particle

105   types present in the troposphere (De Leeuw et al., 2011). Due to their abundance, SSA particles greatly

106   increase the particulate bromide on aerosol surfaces available for heterogeneous reactive bromine

107   chemistry. Debromination of acidified aerosol increases reactive bromine by 30%, although global

108   models may underestimate Arctic reactive bromine when considering only open ocean-sourced SSA

109   (Schmidt et al., 2016). Initial literature on Arctic reactive bromine chemistry identified aerosol particles

110   as a potential saline surface for reactive bromine photochemistry (Fan and Jacob, 1992; Vogt et al., 1996)

111   and field studies confirmed that SSA is depleted in bromide (Ayers et al., 1999; Hara et al., 2018). If one

112   supposes that SSA can only be produced from the open ocean source of SSA, the lack of Arctic Ocean

113   open water during the winter/spring is at odds with observations of high SSA concentrations observed

114   during the winter months in polar regions (Wagenbach et al., 1998; Huang et al., 2018). The formation of

115   SSA from the sublimation of blowing snow particles over the Arctic Ocean was proposed as an alternate

116   SSA production mechanism (Yang et al., 2008, 2010, 2019). Recent field studies have confirmed the

117   direct production of SSA from blowing snow (Frey et al., 2020). A blowing snow SSA mechanism was

118   implemented in the global chemical model GEOS-Chem and was able to explain wintertime SSA

119   enhancements over the Arctic (Huang and Jaeglé, 2017) as well as CALIOP-detected aerosol particle

120   abundance (Huang et al., 2018) and high levels of Arctic BrO detected by satellites in spring (Huang et

121   al., 2020).

122   Snowpack containing bromide salts was also identified as a source of reactive bromine (Tang and

123   McConnell, 1996). Molecular bromine was measured above the snowpack at levels up to 25 pmol/mol

124   (Foster et al., 2001). Field experiments demonstrate that the snowpack emits Br_2, Cl_2, and BrCl, with

125   emission affected by ambient ozone levels, the snowpack ratio of bromide to chloride, and exposure to

126   sunlight (Pratt et al., 2013; Custard et al., 2017). Box modeling found that the flux of reactive bromine

127   from the surface of the Arctic Ocean sea ice is a prerequisite for bromine activation (Lehrer et al., 2004).

128   Box modeling found that both HOBr and $BrNO_3$ can be converted to Br_2 in the snowpack (Wang and

129   Pratt, 2017). Detailed one dimensional models of the snowpack-air interface find that reactive bromine

130   production can occur in the interstitial air between snowpack grains (Thomas et al., 2011; Toyota et al.,

131   2014), with ozone depletion events arising from snowpack reactive bromine production (Thomas et al.,

132   2011; Toyota et al., 2014; Cao et al., 2016). However, a detailed snowpack model coupled to an

133   atmospheric model would be sensitive to important parameters such as snowpack bromide content and

134   acidity of the air-ice interface that are highly variable across the Arctic (Toom-Sauntry and Barrie, 2002;

135   Krnavek et al., 2012). A mechanism to parameterize the release of molecular bromine from snowpack

136   upon deposition of ozone, HOBr, and $BrNO_3$ was implemented in the GEM-AQ model and captured

137   many of the observed features of reactive bromine in the Arctic troposphere (Toyota et al., 2011). The

138   mechanisms from Toyota et al. (2011) assumes a 100% yield of molecular bromine on deposition of

139   HOBr or $BrNO_3$ (see Figure 1 PACK) and a diurnally varying yield of Br_2 on ozone deposition of 7.5%

140   during the daytime (solar elevation angle $> 5°$) and 0.1% during the nighttime (solar elevation angle $< 5°$)

141   (see Figure 1 PACK). In the Toyota et al. (2011) parameterization, the daytime yield of Br_2 from ozone

142   was increased to 7.5% to match surface ozone depletion observations and is based on the assumption that

143   photochemical reactions in the snowpack would trigger a bromine explosion and amplify the net release

144   of Br_2 (Toyota et al., 2011). Herrmann et al (2021) implemented the Toyota et al. (2011) mechanism in

145   WRF-Chem and found snowpack Br_2 production was capable of replicating ozone depletion events

146   observed in multiple datasets. Marelle et al. (2021) implemented a surface snowpack mechanism based on

147   Toyota et al. (2011) and a blowing snow SSA mechanism based on Yang et al. (2008) and Huang and

148   Jaeglé (2017) and found improved prediction of ozone depletion events, the majority of which were

149   triggered by the snowpack mechanism. The Toyota et al. (2011) mechanism was also implemented in the

150   EMAC model and replicated many of the features of reactive bromine events observed by satellite-based

151   GOME sensor (Falk and Sinnhuber, 2018).

152   Field campaigns have directly observed the production of SSA from blowing snow (Frey et al.,

153   2020) as well as production of Br_2 from the snowpack (Pratt et al., 2013) in the environment. This

154   manuscript uses both production mechanisms for the first time in the global chemical model GEOS-

155   Chem. We devised a set of six model runs to test each mechanism individually and together as well as one

156   control run using neither mechanism. We compare BrO simulated in each model run against extensive

157   ground-based observations of BrO made from February to June 2015. This set of modeling scenarios

158   allows identification of the effects of each mechanism on BrO as well as the synergistic effects of both

159   mechanisms working together.

2. Data sources and methods

2.1 MAX-DOAS observation platforms

Multiple axis differential optical absorption spectroscopy (MAX-DOAS) remotely measures the vertical profile of BrO (Hönninger and Platt, 2002; Carlson et al., 2010; Frieβ et al., 2011; Peterson et al., 2015; Simpson et al., 2017). BrO is commonly used as a proxy for total tropospheric reactive bromine (Chance, 1998; Richter et al., 1998; Wagner and Platt, 1998; Theys et al., 2011; Choi et al., 2012). MAX-DOAS instruments were mounted on all of the fifteen floating autonomous platforms (O-Buoys) deployed in the Arctic sea ice as a part of the National Science Foundation-funded Arctic Observing Network project (Knepp et al., 2010). Since MAX-DOAS requires sunlight to operate, measurements are not available in winter. Spring observations on the O-Buoys typically begin in April when there is enough O-Buoy solar power to defrost the MAX-DOAS viewport. Figure 2 shows the O-Buoys active during 2015. O-Buoy 10 was deployed into sea ice in fall 2013 and measured reactive halogen chemistry in spring 2014 and 2015. Most O-Buoys were destroyed in the summer, crushed between fragments of melting sea ice. However, O-Buoy 10 survived summer 2014 in an intact ice floe, survived the winter of 2014-15, and re-started MAX-DOAS observations in April 2015. O-Buoys 11 and 12 were deployed in fall 2014 and also re-started observing BrO in April 2015. Figure 2 shows the GPS-derived tracks of the O-Buoys for their full deployment and highlights the O-Buoy locations from April to June 2015 when the BrO observations considered in this analysis were gathered. A MAX-DOAS instrument of the same design was deployed at the Barrow Arctic Research Center (BARC) on the coast of the Arctic Ocean located at 156.6679°W, 71.3249°N near Utqiaġvik, AK (Simpson, 2018), also shown in Figure 2. Unlike the O-Buoy MAX-DOAS systems, which were powered by batteries and solar panels, the BARC MAX-DOAS was powered from local utilities and was able to defrost its viewport to gather BrO observations earlier in the year, including February and March 2015. The BARC MAX-DOAS data was compared with two O-Buoy style MAX-DOAS instruments deployed on Icelander platforms (deployed on top of sea ice instead of within) and measurements from the various MAX-DOAS systems were found to be comparable (Simpson et al., 2017). The reactive bromine season ends when the BrO slant column densities fall below the instrument detection limit and do not recover, which we call the seasonal end date (Burd et al., 2017). All O-Buoy and BARC (Utqiaġvik) data are available at arcticdata.io (Simpson et al., 2009; Simpson, 2018). More information on the time periods of spring BrO observations can be found in Swanson et al. (2020) and Burd et al. (2017). For comparison to the MAX-DOAS BrO observations, GEOS-Chem model simulations are sampled along the GPS-derived paths of O-Buoys 10, 11 and 12 as well as at BARC.
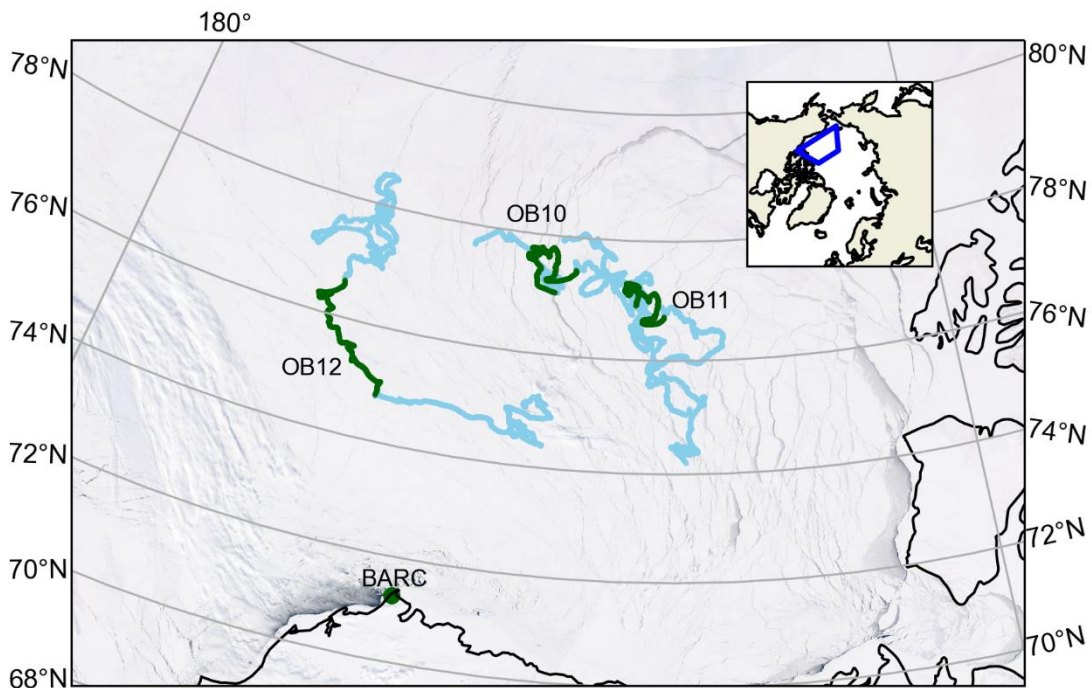
Figure 2: Locations of MAX-DOAS BrO observations used in this work.
Blue lines show the drift tracks of O-Buoys, with green showing the locations with valid BrO
measurements in spring 2015. Location of Barrow Arctic Research Center (BARC) in Utqiaġvik indicated
by green dot. True color MODIS imagery on 1 April 2015 shows typical sea ice coverage (NASA 2015).
Inset map shows location of map grid within northern hemisphere.

2.2 MAX-DOAS profile retrieval

Vertical profiles of BrO were derived from MAX-DOAS observations by means of optimal estimation inversion procedures detailed in Peterson et al. (2015) with settings detailed in Simpson et al. (2017). The HeiPro optimal estimation algorithm (Frieß et al., 2006, 2019) is used to retrieve a vertical profiles of BrO between the surface and 4km from the MAX-DOAS observations. Examination of the averaging kernels from each MAX-DOAS retrieval finds the retrieved vertical profile of BrO is best represented by two quantities: the vertical column density of BrO in the lowest 200 m, and the vertical column density of BrO in the lowest 2000 m of the troposphere referred to in this manuscript as BrO_{LTcol} (Peterson et al., 2015). It was shown in Peterson et al. (2015) that these two quantities were largely independent of each other, were fairly insensitive to variations in the assumed prior profile, and represented the ~2-3 degrees of freedom for signal indicated by the optimal estimation retrieval. An important consideration of this method is that when the visibility is poor, the MAX-DOAS is unable to traverse the lowest 2000m AGL and the BrO_{LTcol} cannot be measured accurately. Therefore, our quality-control algorithm eliminates BrO_{LTcol} observations when the degrees of freedom for signal in the lofted (200m - 2000m AGL) layer were below 0.5 (Simpson et al., 2017). The average fitting error (1σ error) of BrO_{LTcol} during spring 2015 was $5.6*10^{12}$ molecules/cm^2.

2.3 SSA production from open ocean

Seafoam from breaking waves and bursting of bubbles forms aerosol droplets suspended in the marine boundary layer (Lewis and Schwartz, 2004). We calculate emission of sea salt aerosol particles from the open ocean as a function of wind speed and sea surface temperature (SST) using the mechanism initially described in Jaeglé et al. (2011) and updated with decreased emissions over cold (SST < 5°C) ocean waters (Huang and Jaeglé, 2017). Two separate SSA tracers are transported: accumulation mode SSA (r_{dry} = 0.01−0.5 µm) and coarse mode SSA (r_{dry} = 0.5–8 µm). Sea salt bromide is emitted assuming bromine content of $2.11×10^{-3}$ kg Br per kg of dry SSA (primarily NaCl) based on the mean ionic composition of sea water (Sander et al., 2003). Bromide content is tracked separately on accumulation mode SSA and on coarse mode SSA. Freshly emitted SSA is alkaline and can be titrated to a pH of 5 by uptake of acid gases SO_2, H_2SO_4, and HNO_3 (Alexander et al., 2005). Heterogeneous chemical reactions can convert SSA-transported bromide into gaseous reactive bromine species in the atmosphere. We run our open ocean SSA calculations at 0.5° latitude x 0.625° longitude spatial resolution using the harmonized emissions component (HEMCO) for highest possible detail (Keller et al., 2014; Lin et al., 2021) including cold water corrections used in Jaeglé et al. (2011) . Production of SSA from open oceans followed by advection can lead to reactive bromine recycling over Arctic Ocean sea ice. Each of our model runs reads the dataset generated offline by HEMCO rather than spend computational time

230   replicating open ocean SSA emissions. We call our control run using only open ocean SSA emissions

231   BASE.

2.4 Blowing snow SSA production

233   Snow can be lofted from the snowpack into the lowest layers of the troposphere by high wind

234   speeds, where it can undergo saltation (bouncing leading to fragmentation) and sublimation to form SSA

235   (Yang et al., 2008, 2010; Frey et al., 2020). This process is modeled as a function of humidity, ambient

236   temperature, wind speed, snow particle size distribution, and the salinity of the blowing snow (Yang et

237   al., 2008, 2010). We assume that snowpack exists on all sea ice surfaces during the Arctic Spring after

238   snow accumulation during winter on sea ice of all ages. Three thresholds must be met for SSA production

239   from blowing snow (Dery and Yau, 1999; Déry and Yau, 2001). A temperature threshold restricts SSA

240   production from blowing snow to temperatures below freezing. The humidity threshold is based on

241   relative humidity with respect to ice. Sublimation from snow crystals cannot occur if the air is saturated,

242   and no SSA is produced if RH_{ice} is greater than 100%. The wind speed threshold requires 10-m wind

243   speed to be greater than a threshold value defined in Equation 1 for any production of SSA (Dery and

244   Yau, 1999; Déry and Yau, 2001).

245     $$U_t = 6.975 + 0.0033(T_s + 27.27)^2 \tag{1}$$

246   The wind speed threshold (U_t) is dependent on surface temperature (T_s) in Celsius with a minimum

247   threshold of 6.975 m/s at -27.27 °C and a maximum threshold at 0 °C of 9.429 m/s. The 10-m wind speed

248   threshold is the most stringent and often controls the production of SSA from blowing snow.

249   Production of blowing snow SSA is highly sensitive to surface wind speed. We use the highest

250   resolution surface wind speed dataset to ensure the most accurate modeling of SSA and reactive bromine.

251   The MERRA-2 Global Reanalysis Product has a 0.5° latitude x 0.625° longitude resolution which is

252   typically re-gridded to a lower resolution for global chemical modeling. Previous use of the snowpack

253   blowing snow SSA mechanism used MERRA-2 data re-gridded to either 2°x2.5° or 4°x5° latitude and

254   longitude (Huang and Jaeglé, 2017; Huang et al., 2018, 2020). Re-gridding to coarser spatial resolution

255   may smooth out the highest 10-m wind speeds by averaging them with lower wind speeds in the grid cell.

256   The Utqiaġvik MERRA-2 10-m wind speeds at different spatial resolutions are shown in Supplemental

257   Figures S1, S2 and S3 to illustrate this effect. Average Utqiaġvik 10-m wind speeds for 2015 are 5.3 m/s

258   at 2°x2.5° resolution and 5.5 m/s at 0.5°x0.625° resolution. The maximum Utqiaġvik 10-m wind speed at

259   MERRA-2 2x2.5 is 16.3 m/s, while the maximum wind speed at MERRA-2 0.5°x0.625° is 19.3 m/s.

260   These extremely high wind speed events are more common at higher spatial resolution and can contribute

261   an outsized amount of SSA to the marine boundary layer. Supplemental Figure S4 shows the measured

262   10-m wind speed at BARC, along with daily average threshold wind speed (Equation 1). Spikes in daily

263 averaged wind speed at BARC in April can contribute to SSA formation and justify the use of high-
264 resolution MERRA-2 wind speed data.

265   Snow salinity is influenced by snow age and the material underlying the snow (Krnavek et al.,
266 2012). The median surface snowpack salinity near Utqiaġvik was measured at 0.67 practical salinity units
267 (PSU) for 2-3 weeks old sea ice, 0.12 PSU for thicker first year ice, and 0.01 PSU for multi-year ice
268 (MYI) (Krnavek et al., 2012). Snow salinity is also a function of snow depth above sea ice, with blowing
269 surface snow having much lower salinity than snow at depth that is in contact with the sea ice (Frey et al.,
270 2020). Domine et al**.** (2004) measured median salinity at 0.1 PSU on snowpack over first year ice and
271 0.02 on snowpack over multi-year ice. In this analysis we use a salinity of 0.1 PSU on first-year sea ice as
272 in Huang et al. (2020). The production of reactive bromine from sea ice types is entirely dependent on
273 PSU in this parameterization. Previous modeling efforts have used 0.01 PSU for MYI (Huang et al.,
274 2018) and underestimate BrO production in high Arctic areas with increased MYI coverage. The bromide
275 content of surface snow over MYI is enriched by deposition of SSA and trace gases, and MYI regions
276 may play a role in springtime halogen chemistry (Peterson et al., 2019). Previous analysis of O-Buoy data
277 found no statistically significant differences in springtime BrO between regions of the Arctic (Swanson et
278 al., 2020). We use 0.05 PSU for snowpack on MYI as in Huang et al. (2020).

279   Another important parameter for SSA formation is the number of SSA particles formed from each
280 blowing snowflake. A value of 5 particles per snowflake was used in Huang and Jaeglé (2017) based on
281 wintertime observations of supermicron and sub-micron SSA at Barrow. Values of 1 and 20 particles per
282 snowflake have been tested (Yang et al., 2019) but it was unclear which value was more realistic. We use
283 a particle formation value of 5 particles per snow grain as in Huang et al. (2020).

284   Snowpack may be enriched or depleted in bromide compared to seawater, which is thought to be
285 an effect of atmospheric deposition or release of bromine from snowpack (Krnavek et al., 2012).
286 Snowpack enrichment due to atmospheric deposition is less pronounced when snowpack salinity is high,
287 with snowpack containing 1000 μM Na^+ (approximately 0.06 PSU) or more never exceeding twice the
288 seawater ratio of bromine to chloride (Krnavek et al., 2012). Domine et al. (2004) found an increased
289 enrichment factor of five times seawater in snow with a salinity of 100 μM Cl^- (approximately 0.006
290 PSU). We use a snowpack enrichment factor of bromide five times that of seawater as in Huang et al.
291 (2020) where this enrichment best agreed with GOME-2 observations. However, we note that a bromide
292 enrichment factors five times seawater exceeds enrichment factors of two measured in snowpack with a
293 salinity of 0.1 PSU (Krnavek et al., 2012).

294   Our choice of model input settings is similar to Huang et al. (2020) but we will be running the

295   blowing snow SSA mechanism in HEMCO at a 0.5° latitude x 0.625° longitude spatial resolution. The

296   model run using the results of our high-resolution blowing snow SSA HEMCO simulation is called

297   BLOW.

298   **2.5 Snowpack emissions of molecular bromine**

299   We base our Br_2 emissions scheme on Toyota et al. (2011) and Marelle et al. (2021), which

300   prescribe a yield of Br_2 upon snowpack deposition of ozone, $BrNO_3$ and HOBr. In other modeling studies,

301   this simplified deposition-based mechanism captured the synoptic-scale behavior of reactive bromine

302   production across the Arctic (Toyota et al., 2011; Falk and Sinnhuber, 2018; Herrmann et al., 2021;

303   Marelle et al., 2021). These modeling studies used different yields of Br_2 upon deposition over land

304   snowpack, multi-year ice, and first year ice, restricting the production of molecular bromine from ozone

305   deposition to first year ice surfaces. None of these studies were coupled to a snowpack model tracking

306   snow bromide, and effectively assume an infinite bromide reservoir with Br_2 production limited only by

307   the deposition flux and Br_2 yield.

308   Field studies indicate that snowpack over multi-year ice, first-year ice, and land regions may

309   contribute to reactive bromine chemistry. Krnavek et al. (2012) found snow bromide content spanning six

310   orders of magnitude, with individual samples taken from multi-year ice, first-year ice, and land regions

311   showing variability of up to three orders of magnitude for each region. Analysis of variance in

312   tropospheric BrO from 2011-2016 found no statistically significant differences in tropospheric BrO

313   between different regions of the Arctic (Swanson et al., 2020). Both coastal snowpack and multi-year ice

314   regions may produce reactive bromine. Molecular bromine production has been observed from coastal

315   snowpack on exposure to ozone (Pratt et al., 2013; Custard et al., 2017). Airborne sampling has observed

316   enhanced BrO up to 200 km inland (Peterson et al., 2018). Snow above multi-year sea ice regions is

317   depleted in bromide, indicating that it may play a role in Arctic bromine chemistry (Peterson et al., 2019).

318   Our modeling study tests the hypothesis that all snow has a uniform ability to produce molecular

319   bromine, effectively assuming an infinite bromide reservoir with Br_2 production limited only by the

320   deposition flux. We differ from previous model parameterizations in allowing uniform Br_2 production

321   upon snowpack deposition of ozone, $BrNO_3$ and HOBr over all sea ice surfaces and selected coastal

322   snowpack regions. We only allow snowpack Br_2 production when the surface temperature is below

323   freezing. Surface temperatures may rise above freezing and drop back below freezing in the Arctic spring,

324   which may allow for snowpack Br_2 to simulate late-season bromine production events after snowpack

325   melt such as those observed in Burd et al. (2017). We expect higher predictions of snowpack molecular

326 bromine production than recent modeling efforts (Herrmann et al., 2021; Marelle et al., 2021) in which

327 ozone deposition over land and multi-year ice surfaces did not produce molecular bromine.

2.5.1 Snowpack Br_2 production over sea ice

329   We assume a uniform production of Br_2 on deposition to snowpack over oceanic ice whether the

330 ice is first-year sea or multi-year sea ice. We use MERRA-2 fractional ocean ice coverage fields, which

331 introduces some artifacts. MERRA-2 classifies the freshwater Great Lakes as ocean, but sea ice and

332 snowpack on those frozen lakes is unlikely to have sufficient bromide to support large Br_2 fluxes due to

333 its distance from the ocean. Therefore, we specifically prohibit snowpack Br_2 emissions in the Great

334 Lakes region (between 41° N and 49° N latitude and 75° W and 93° W longitude). This choice is in

335 agreement with McNamara et al. (2020), who found road salt derived aerosol particles are responsible for

336 80-100% of atmospheric $ClNO_2$ in Michigan with no strong indication for a source of reactive halogens

337 from nearby Great Lakes.

2.5.2 Snowpack Br_2 production over land

339   We wish to only enable production of Br_2 over land if the snowpack is sufficiently enriched in

340 bromide. Snowpack over land surfaces and glaciers may be enriched in bromide by oceanic SSA sources

341 (Jacobi et al., 2012, 2019). The distance that SSA may be transported inland from the coast is limited by

342 geographical features such as mountains. Based on direct observations of reactive bromine chemistry up

343 to 200 km from the Alaskan coastline (Peterson et al., 2018), we include unlimited production of Br_2 from

344 specific land grid cells within 200 km of the coast upon deposition of ozone, HOBr, and $BrNO_3$. We only

345 allow the fraction of each grid cell that is within 200 km of the coastline (Group and Stumpf, 2021) to

346 produce molecular bromine. We further restrict snowpack Br_2 emissions to locations that are less than 500

347 m above sea level, because higher elevation locations are unlikely to be enriched by sea spray. This

348 altitude screen eliminates Br_2 emissions from coastal mountains such as the Alaskan Rockies, the Brooks

349 Range in Alaska, and the Scandinavian Mountains as well as from the Greenland Plateau. Halogen

350 chemistry may occur over the Greenland ice sheet (Stutz et al., 2011) contrary to this screen, but this will

351 have minimal impact on the regions of interest in this manuscript.

352   Our final screen is based on the average snow depth in each land grid cell. Both modeling studies

353 (Thomas et al., 2011; Toyota et al., 2014) and field studies (Domine et al., 2004; Pratt et al., 2013;

354 Custard et al., 2017; Frey et al., 2020) agree that bromine chemistry can occur in the better ventilated and

355 illuminated top of the snowpack. Regions with less than 10 cm of snowpack may not have sufficient

356 snow for reactive bromine chemistry, thus we only produce snowpack Br_2 when the average snow depth

357 in a land grid cell is 10 cm or greater. This filter prevents molecular bromine production in the lower

358 latitude regions with minimal snow coverage and is necessary because ozone deposition to plants in

359 snow-free grid cells often exceeds the slow deposition of ozone to snowpack and would not be expected

360 to produce Br_2.

2.5.3 Diurnal yield of Br_2 on ozone deposition

362   We choose two alternate assumptions for the yield of Br_2 during the day. Toyota et al. (2011)

363 initially assumed a constant yield of Br_2 from ozone deposition of 0.1% based on laboratory observations

364 of nighttime bromine activation on ozone deposition (Oum et al., 1998; Wren et al., 2010, 2013) and then

365 adjusted the daytime yield of Br_2 on ozone deposition to 7.5% to better match surface ozone mixing ratios

366 measured at coastal stations. This increased daytime yield value was chosen based on the assumption that

367 photochemistry may trigger an autocatalytic cycle leading to a 75-fold increase in Br_2 yield. The

368 PHOTOPACK runs uses the increased daytime Br_2 yield of 7.5% when the solar elevation angle is 5° or

369 greater. Previous implementations of the snowpack mechanism (Toyota et al., 2011; Herrmann et al.,

370 2021; Marelle et al., 2021) predict ozone deposition velocities over Arctic sea ice on the order of 0.01

371 cm/s. Their findings agree with a modeling sensitivity study finding best agreement with observations

372 using ozone deposition rates between 0.00-0.01 cm/s (Helmig et al., 2007). Our model predicts similar

373 polar open ocean ozone deposition rates of 0.009 cm/s (Pound et al., 2020) but predicts higher modeled

374 deposition velocity of ozone over Arctic sea ice between 0.02 cm/s and 0.1 cm/s based on the month (see

375 Supplemental Figure S5), with higher values influenced by proximity to the coast as observed along non-

376 Arctic coastlines in Bariteau et al. (2010). Thus, our PHOTOPACK run may predict much higher Br

377 emissions than previous snowpack predictions despite the same yield values due to differences in

378 deposition. To match our magnitude of Br_2 production with previous implementations of the snowpack

379 mechanism (Toyota et al., 2011; Herrmann et al., 2021; Marelle et al., 2021) we add two PACK runs with

380 a constant Br_2 yield on ozone deposition of 0.1% based on yield values in Toyota et al. (2011). Both

381 PACK and PHOTOPACK runs assume 100% conversion of deposited HOBr and $BrNO_3$ to Br_2. Table 1

382 shows further model run yield details.

Table 1 Model run settings

384 Sea salt aerosol particles are produced from blowing snow as detailed in Section 2.5. Daytime is defined
385 as when the solar elevation angle is greater than 5°, nighttime is defined as when the solar elevation angle
386 is less than 5°.

Model Run	Blowing snow SSA produced	Millimoles Br yielded per mole O3 deposited (daytime)	Millimoles Br yielded per mole O3 deposited (nighttime)
BASE	FALSE	0	0
BLOW	TRUE	0	0
PACK	FALSE	1	1
BLOW+PACK	TRUE	1	1

PHOTOPACK	FALSE	75	1
BLOW+PHOTOPACK	TRUE	75	1

387

2.6 GEOS-Chem chemistry and transport model

389   The GEOS-Chem global atmospheric chemistry and transport model (Bey et al., 2001) simulates

390 emissions, transport, and chemistry of atmospheric trace gases and aerosols, including halogens. The

391 chemical mechanism in GEOS-Chem 12.9.3 (http://www.geos-chem.org, last access 29 October 2019,

392 DOI:10.5281/zenodo.3974569) includes HO_x-NO_x-VOC-O_3-halogen-aerosol tropospheric chemistry

393 (Mao et al., 2013; Fischer et al., 2014; Fisher et al., 2016; Travis et al., 2016; Wang et al., 2021). The

394 model has been regularly and consistently updated to reflect current understanding of heterogeneous and

395 gas-phase halogen chemistry.

396   Halogens in the troposphere may be sourced from photooxidation of halocarbons, emissions of

397 iodine from the ocean surface, downward transport of halogens from the stratosphere, and release of

398 halogens through heterogeneous chemistry on SSA. Figure 1 shows a simplified version of the GEOS-

399 Chem reaction scheme focusing on tropospheric bromine reactions and reservoirs. Heterogeneous

400 reactions for release of reactive bromine from aerosol surfaces were added to GEOS-Chem (Parrella et

401 al., 2012) and have been updated to include multiphase reactions involving cloud aerosols, cloud droplets,

402 and ice aerosols as well as inter-halogen reactions between bromine, chlorine and iodine species (Schmidt

403 et al., 2016; Sherwen et al., 2016a; Wang et al., 2019b) and input from the stratosphere (Eastham et al.,

404 2014). Recent updates also include reactions between sulfur (IV) species and HOBr, which lead to a 50%

405 decrease in Br_y due to the scavenging of HOBr on aerosol surfaces containing sulfur (Chen et al., 2017).

406 These HOBr-sulfur(IV) reactions are critical in moderating tropospheric BrO in the mid latitudes (Zhu et

407 al., 2019). In GEOS-Chem 12.9 the halogen chemical mechanism was modified extensively to include

408 chlorine chemistry as detailed in Wang et al. (2019b) with updated halogen-sulfur (IV) rates (Liu et al.,

409 2021), reaction of S(IV) + HOCl, and improved cloud pH calculation from Shah et al. (2020). For the

410 simulations here, GEOS-Chem uses the Modern-Era Retrospective Analysis for Research and

411 Applications, version 2 (MERRA-2) assimilated meteorological fields (Gelaro et al., 2017) re-gridded

412 from native resolution of 0.5°x0.625° latitude and longitude to 2°x2.5° using a reduced vertical grid of 47

413 layers.

414   We initialize our model in October 2014 from a full-chemistry benchmark file, allowing for 6

415 months of spin up before our period of interest spanning from March to November 2015. We run six

416 different model simulations with settings detailed in Table 1. The base model (BASE) includes the

417 halogen sources described above but no Arctic-specific halogen sources. The BLOW simulation adds

418   SSA production from blowing snow following Huang et al (2020) but using a more recent version of

419   GEOS-Chem. The PACK simulation adds snowpack Br_2 emissions using a constant yield from O_3

420   deposition. The PHOTOPACK simulation also emits Br_2 from snowpack but increases the Br_2 yield from

421   O_3 deposition under sunlight. These blowing snow SSA and snowpack sources are combined in the

422   BLOW+PACK and BLOW+PHOTOPACK simulations.

423   **2.7 Comparing GEOS-Chem results to MAX-DOAS vertical column densities**

424   GEOS-Chem simulates BrO mixing ratios for each of its 47 atmospheric layers. Reducing the

425   vertical resolution of the more-resolved GEOS-Chem predictions to be comparable to the coarser MAX-

426   DOAS data is necessary for appropriate comparison (Rodgers and Connor, 2003). To compare the

427   GEOS-Chem profiles with these two grid-coarsened quantities, we grid-coarsen the averaging kernels

428   produced by the HeiPro retrieval algorithm using Supplemental Equation S1 from Payne et al. (2009) to

429   the partial column averaging kernels shown in Figure 3. We use the average of all April averaging kernels

430   that pass our quality criteria (>0.5 DOFS in the lofted layer), which generally represents non-cloudy

431   conditions. We calculate modeled BrO_{LTcol} by applying the partial column averaging kernels shown in

432   Figure 3 to the GEOS-Chem modeled vertical BrO profiles.

433   Figure 3 shows the average partial column averaging kernel for the surface layer (0-200m AGL)

434   has near unit sensitivity to BrO at the ground, decaying to about 0.5 at 200m AGL then to zero at about

435   400m AGL, as desired. The sensitivity of the BrO_{LTcol} is near unity from about the surface to 600m AGL,

436   then slowly decays with 0.5 sensitivity at 2000m AGL. The resulting sensitivity to mid-tropospheric BrO

437   means that free-tropospheric BrO produced by the GEOS-Chem model contributes to modeled BrO_{LTcol},

438   albeit at 50% or lower sensitivity, even if the GEOS-Chem-predicted free-tropospheric BrO is above the

439   nominal 2000m top of the integration window. The residual sensitivity of the BrO_{LTcol} averaging kernel

440   above 2000m is caused by the limited ability of ground-based MAX-DOAS to distinguish the true altitude

441   of BrO at non-tangent geometries (higher viewing elevation angles) that are required to view BrO at these

442   higher altitudes. Figure 3 shows that BrO above 4 km makes only a small contribution to the modeled

443   BrO_{LTcol}, which was not included in the BrO_{LTcol}.

444
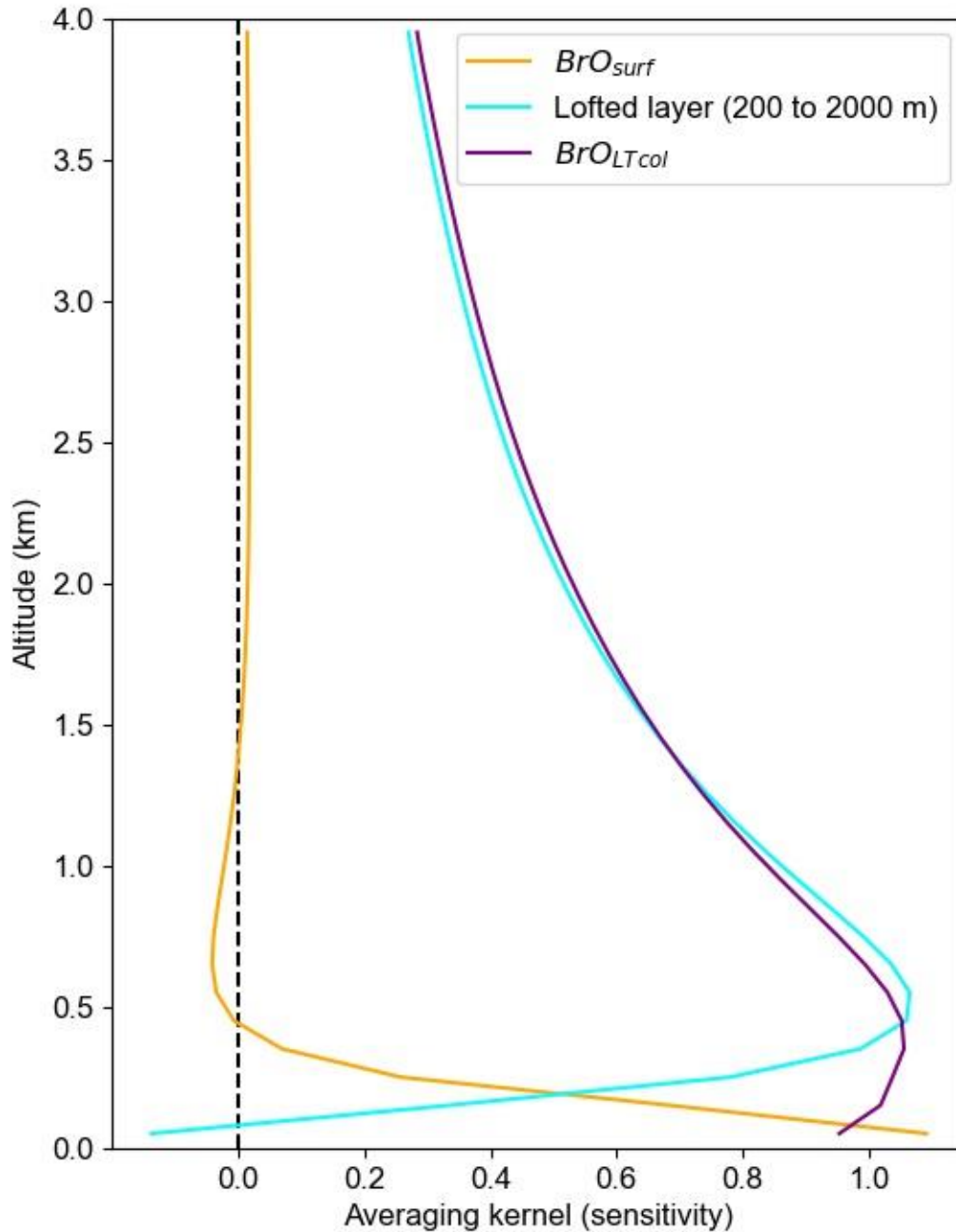
Figure 3: Averaging kernels showing the sensitivity of retrieved BrO$_{LTcol}$ and retrieved BrO$_{surf}$ to

BrO at a range of altitudes.

Each line represents a row of the averaging kernel matrix. BrO$_{surf}$ is the column from the surface to 200 m

and BrO$_{LTcol}$ is the column up to 2000 m.

Although it has been suggested in the literature (von Clarmann and Glatthor, 2019) that averaged

averaging kernels can cause problems, we do not report data when there are clouds and thus are only

using the more consistent averaging kernels that occur under clear sky conditions. We use other criteria

related to vertical visibility to identify clear skies. As described in Peterson et al. (2015), the information

content (DOFS) in the lofted layer is nearly linearly related to the aerosol optical depth.   We find that the

454 slant column density of the O_2-O_2 collisional dimer (aka O_4) observed at 20° elevation angle is correlated

455 with the lofted DOFS (Supplemental Figure S6). From this correlation we find that observations of clear

456 sky conditions have 20° elevation angle O_4 dSCD > 10^{43} molecule^{2}cm^{-5} and use this cut to distinguish

457 clear sky versus clouds. To assure that GEOS-Chem results are only compared to the clear-sky

458 observational data, we apply this clear sky screen to the measured BrO_{LTcol} timeseries. The use of this

459 screen also assists in minimizing variability in the averaging kernels and thus allowing the April averaged

460 partial column averaging kernels (Figure 3) to be applied for clear skies at any time of the year.

461
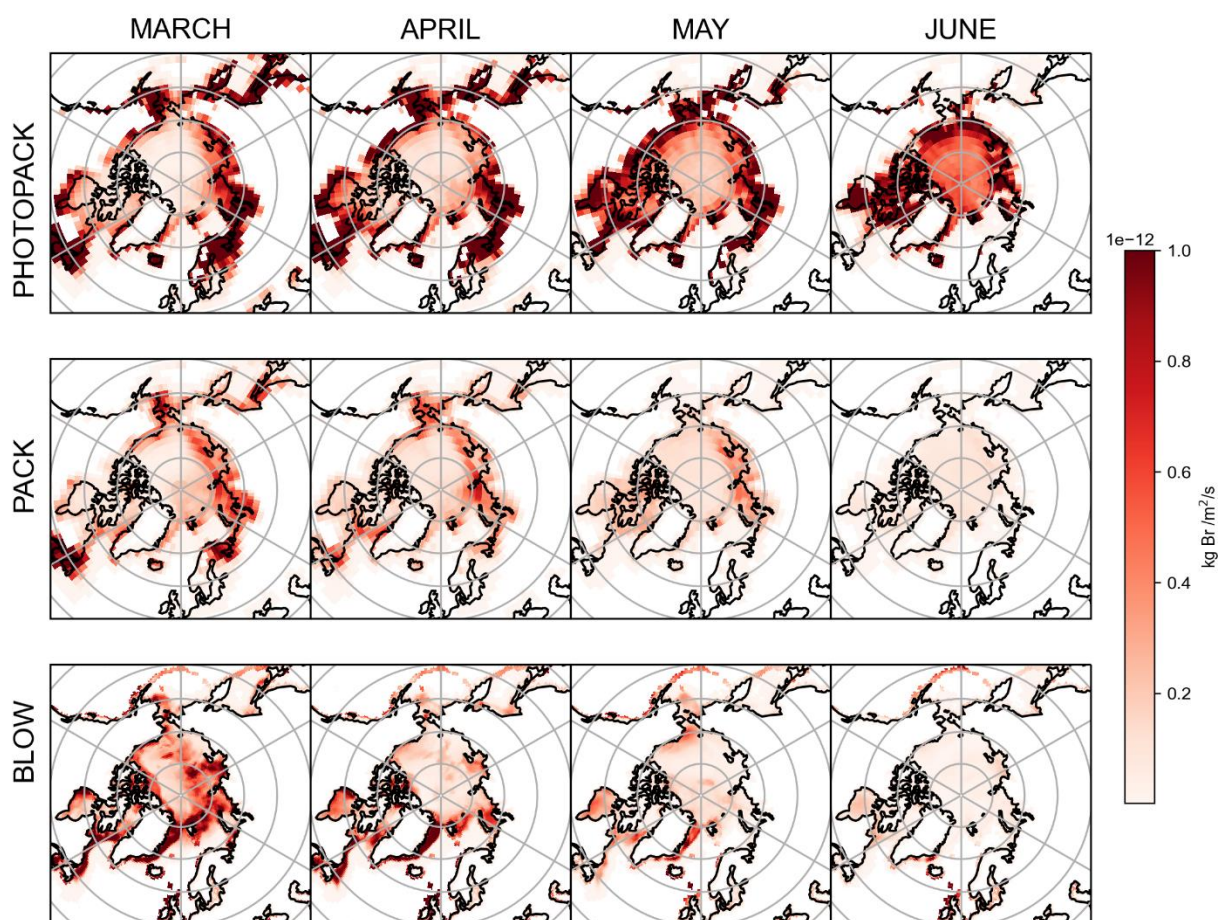
Figure 4: Mean snowpack Br$_2$ and p-Br$^-$ emissions by month, as simulated by GEOS-Chem.
The top row shows emissions of Br$_2$ in the PHOTOPACK run, the middle row shows the emissions of
Br$_2$ in the PACK run, and the bottom row shows emissions of p-Br$^-$ from adding the BLOW mechanism.

3. Examining reactive bromine in the Arctic spring

3.1 Snowpack Br$_2$ emissions

467   The top two rows of Figure 4 shows PHOTOPACK and PACK average snowpack Br$_2$ emissions

468 for each spring month. The emission of Br$_2$ in PHOTOPACK increases over the Arctic Ocean in May and

469   June, when the sun is above the horizon for up to 24 hours per day and ozone deposition yield is almost

470   always at the photo-enhanced level of 7.5%. Notably, Br_2 emissions over the Arctic Ocean in the

471   PHOTOPACK and BLOW+PHOTOPACK runs are highest in June when the sun is nearly always five

472   degrees above the horizon and surface temperatures may drop below freezing. The PACK emissions are

473   lower than the PHOTOPACK Br_2 emissions by an order of magnitude and shows a seasonal cycle with a

474   high BrO_{LTcol} in April and May with a decrease in May and June. While our ozone deposition velocities

475   (see Supplemental Figure S5) over Arctic sea ice are much higher than previous estimates of an

476   approximate magnitude of 0.01 cm/s (Toyota et al., 2011), the PHOTOPACK run highlights that a 75-

477   fold increase in daytime Br_2 yield can lead to predictions of increased Br_2 production over the North Pole

478   in June. Monthly satellite observations show that BrO reaches a minimum over the Arctic Ocean in June

479   (Richter et al., 1998).

480   Coastal land regions within 200 km of the coastline have some of the highest modeled snowpack

481   Br_2 emissions (see Figure 4 rows 1 and 2). Within GEOS-Chem, deposition rates are greatest over land,

482   less rapid over ice-covered ocean, and lowest over open ocean (see Supplemental Figure S5). Lower dry

483   deposition velocities over the ice-covered Arctic Ocean lead to decreased deposition and conversion to

484   Br_2. In GEOS-Chem, ozone mixing ratios and deposition are over three orders of magnitude larger than

485    $BrNO_3$ and HOBr mixing ratios and deposition over the Arctic Ocean, and ozone deposition contributes

486   more than half of total Br_2 emitted in the PACK and BLOW+PACK runs. Our snowpack mechanism

487   assumes that all ozone deposited to the surface of a grid cell reacts with the snowpack cover, with those

488   reactions yielding a set percentage of Br_2. This assumption is more appropriate in the barren snow-

489   covered coastal tundra but may be less accurate in areas where deposition to vegetation dominates. This

490   nonconservative approach may lead to overestimation of Br_2 emissions from snowy vegetated surfaces.

491   Our screens for snowpack emissions described in section 1.3.5 tried to minimize these effects but may not

492   work perfectly due to finite grid cell resolution and other challenges. Increased Br_2 emissions observed in

493   Figure 4 in northern Europe may also be partially driven by increased local mixing ratios of ozone and

494   NO_x over industrialized regions such as the Kola Peninsula.

495   **3.2 Blowing snow aerosol bromide emissions**

496   The bottom row of Figure 4 shows the total quantity of particulate bromide released by the

497   blowing snow SSA mechanism in the BLOW runs. Emissions over the Arctic Ocean decline each month

498   after the March maximum as rising temperatures increase the wind speed threshold for blowing snow

499   SSA production. Some icy coastal regions with frequently high wind speeds such as the Aleutian Islands

500   south of Alaska and the eastern coast of Greenland continue to emit SSA p-Br^- in April, and the extremely

501   high winds in the Aleutians enable SSA production into May. The location of specific high-wind storm

502 systems in spring 2015 may be evident in the darker red spots over the Arctic Ocean, which are

503 particularly noticeable over the Eurasian and Central Arctic in March. These monthly averages are only

504 accurate for the months in spring 2015 and may not be spatially representative of blowing snow SSA

505 production in other years.

506   The impact of the blowing snow SSA emissions on measured BrO is minimal on O-Buoys in the

507 Beaufort Gyre, possibly due to the spatial and seasonal variations in SSA p-Br$^-$ emissions. Figure 4 shows

508 that 2015 SSA production was highest in March and April on the Eurasian and Central sector of the

509 Arctic, and thus the O-Buoys deployed as shown in Figure 2 are less exposed to the effects of SSA

510 production than the Arctic as a whole. Particulate bromide must be activated from SSA by heterogeneous

511 reactions as in Figure 1 and Table 3, leading to photochemical cycles that sustain further activation of

512 bromide from SSA. The dearth of sunlight over the Arctic Ocean in early March coincides with the

513 greatest SSA p-Br$^-$ production and means that the increased February SSA p-Br$^-$ emissions may not lead to

514 a direct increase in BrO.

515 **Table 2: Model root mean square error by run and location.**

516 Root mean squared model error (RMSE) shown in BrO$_{LTcol}$/10^{12} molec/cm^2 RMSE calculated as the

517 square root of the mean of the squared errors for all times with valid observed BrO$_{LTcol}$ in Spring 2015.

Units in BrO$_{LTcol}$./10^{12} molec/cm^2	OB10	OB11	OB12	Utqiaġvik
BASE	9.9	12.9	22.9	13.0
BLOW	9.7	12.7	22.4	12.5
PACK	9.9	10.0	18.6	15.2
BLOW+PACK	10.1	10.1	15.7	17.5
PHOTOPACK	30.0	24.8	26.2	30.1
BLOW+PHOTOPACK	30.3	24.6	26.3	31.4

518

519

520
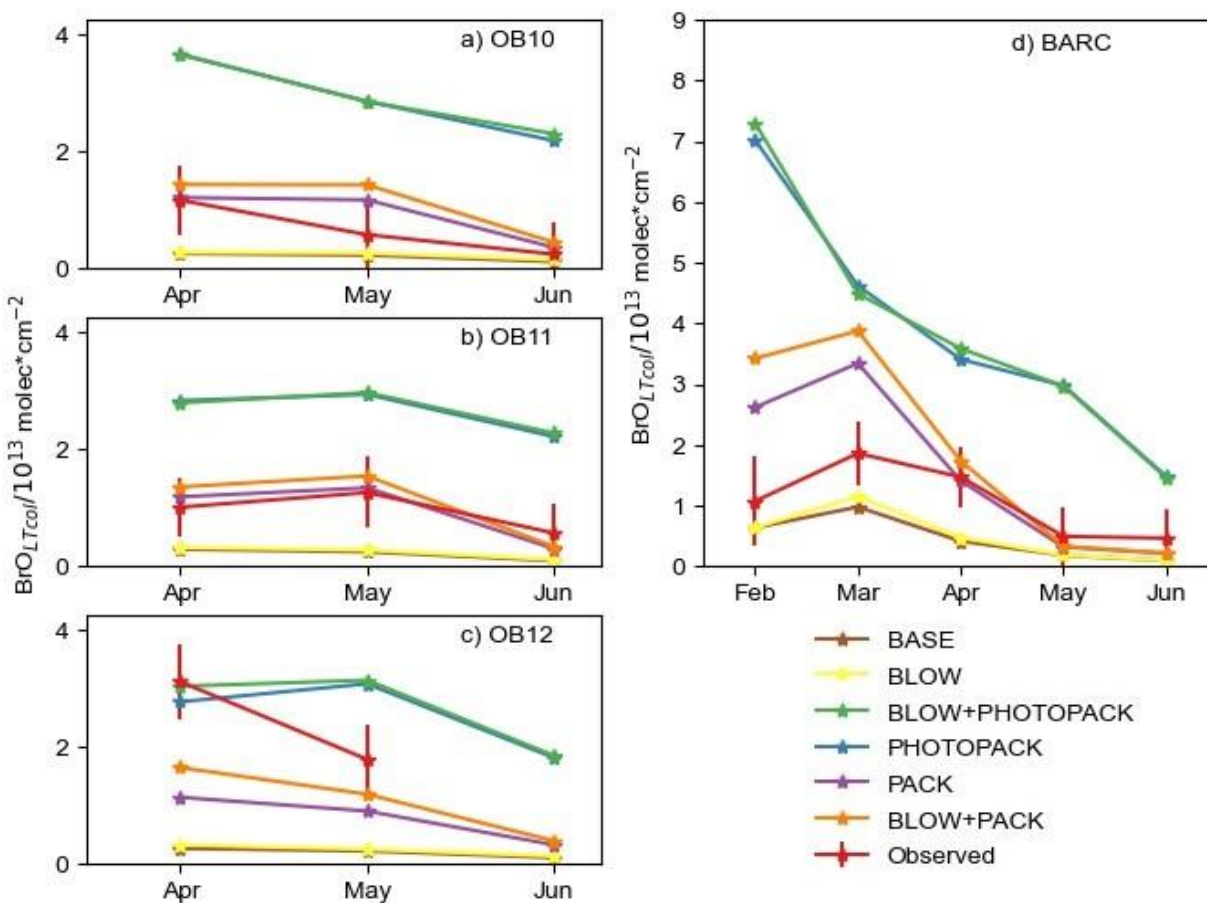
Figure 5: Monthly average BrO$_{LTcol}$ in observations and model

Monthly averages of BrO at a) O-Buoy 10, b) O-Buoy 11, c) O-Buoy 12, and d) BARC at Utqiaġvik only using predictions and observations when dSCDO$_4$ >1*10^{43} molecules^{2}cm^{-5}. Observations with average 1σ error shown in red. All units in 10^{13} molecules/cm^2.

3.3 Snowpack Br$_2$ emissions have more impact than blowing snow SSA on monthly BrO abundance

Increased levels of bromine have been historically seen at Utqiaġvik during February, March, April and May (Berg et al., 1983). Previous O-Buoy data analysis noted BrO dropping to zero in June (Burd et al., 2017). Figure 5 shows monthly averaged modeled BrO$_{LTcol}$ at Utqiaġvik and on the O-Buoys for each model configuration. The difference in GEOS-Chem modeled monthly averaged BrO$_{LTcol}$ for O-Buoys is minimal between the BASE and BLOW runs, the PHOTOPACK and BLOW+PHOTOPACK runs, and the PACK and BLOW+PACK runs. Both BASE and BLOW runs predict near-zero BrO$_{LTcol}$ on all O-Buoys and during most months at Utqiaġvik. The exception to this is the slight increases in monthly modeled BrO$_{LTcol}$ to 1*10^{13} molecules/cm^2 in March and April. This BASE increase in BrO$_{LTcol}$ indicates that oceanic SSA rather than blowing snow SSA can affect modeled BrO at Utqiaġvik due to its closer

536 proximity to open ocean regions than the O-Buoys. The increases in BrO from the BASE model due to
537 the addition of BLOW, most evident at Utqiaġvik in March 2015, are a result of increased particulate
538 bromide available for activation on aerosol surfaces. The PACK and BLOW+PACK runs show the
539 highest skill in reproducing observations, falling within the monthly average of hourly measured BrO_{LTcol}
540 error for 9 of the 13 months plotted in Figure 5. Both PACK and BLOW+PACK replicate the observed
541 monthly pattern especially well on O-Buoy 11 and at Utqiaġvik. Both runs replicate the seasonal pattern
542 of maximum modeled BrO_{LTcol} at Utqiaġvik in March followed by a decrease to near-zero modeled
543 BrO_{LTcol} in May despite model overprediction of BrO_{LTcol} in February and March. The BLOW+PACK
544 monthly BrO_{LTcol} is between $1*10^{12}$ molecules/cm^2 and $1*10^{13}$ molecules/cm^2 higher than PACK monthly
545 BrO_{LTcol} due to the addition of blowing snow SSA. This increase is most pronounced in February and
546 March at Utqiaġvik when lower temperatures lead to lower threshold wind speeds and increased SSA
547 production (see Supplemental Figure S4).

548 The inclusion of increased daytime yield of snowpack Br$_2$ drives monthly average BrO_{LTcol} above
549 $3*10^{13}$ molecules/cm^2 in the PHOTOPACK and BLOW+PHOTOPACK runs from February until June,
550 far above peak observed monthly BrO_{LTcol} of $2*10^{13}$ molecules/cm^2. The PHOTOPACK and
551 BLOW+PHOTOPACK runs show steady decline in BrO_{LTcol} from February to June at Utqiaġvik.
552 Predictions of PHOTOPACK and BLOW+PHOTOPACK monthly June BrO_{LTcol} above $2*10^{13}$
553 molecules/cm^2 on the O-Buoys is due to increasing photo-assisted local snowpack Br$_2$ emissions over the
554 Arctic Ocean (see Figure 5). The PHOTOPACK mechanism predicts monthly average BrO_{LTcol} within
555 observational error only on O-Buoy 12 in April. Aside from this replication of the sparsely sampled O-
556 Buoy 12 April BrO_{LTcol}, the PHOTOPACK mechanism overestimates BrO_{LTcol}.

557 Table 2 shows the root mean squared error (RMSE) of each model run as compared to BrO_{LTcol}
558 observations in at each different location in Spring 2015. The PACK and BLOW+PACK runs have the
559 lowest RMSE on O-Buoys 11 and 12, and among the lowest RMSE on O-Buoy 10. Utqiaġvik shows the
560 lowest RMSE of $1.25*10^{13}$ molec/cm^2 for the BLOW run, although the PACK run is not too far off at
561 $1.57*10^{13}$ molec/cm^2. Despite the fact that BLOW+PACK has a higher RMSE of $1.75*10^{13}$ molec/cm^2 at
562 Utqiaġvik, the BLOW+PACK run performs the best or near the best of all runs on the O-Buoys and
563 includes both known processes for Arctic reactive bromine production. The PHOTOPACK and
564 BLOW+PHOTOPACK runs with increased daytime yield have a consistently high RMSE of $2.46*10^{13}$
565 molec/cm^2 or higher, often double the RMSE of other model runs.

566
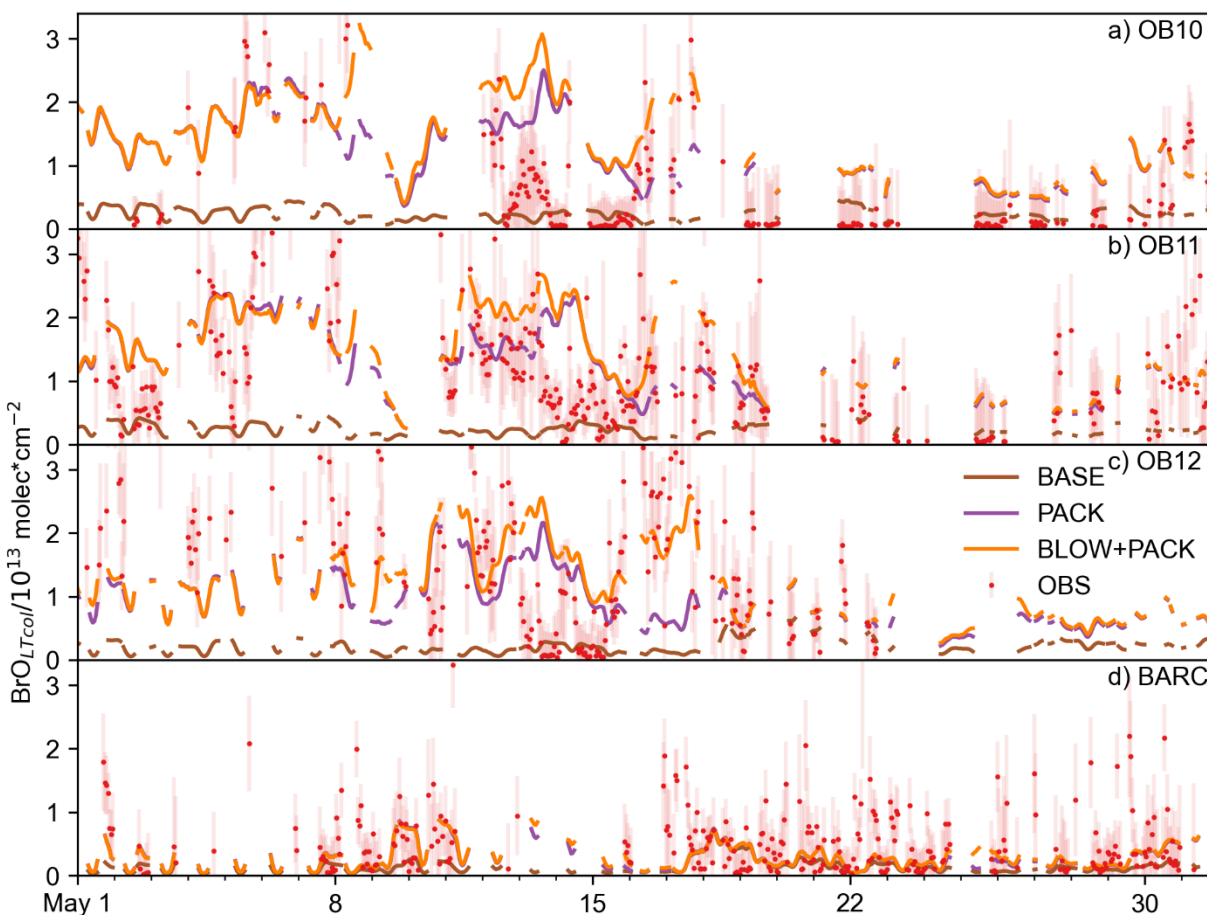
568
569 **Figure 6: May Hourly BrO$_{LTcol}$ timeseries**
570 Hourly timeseries of BLOW+PACK, PACK, and BASE BrO$_{LTcol}$ on a) O-Buoy 10, b) O-Buoy 11, c) O-
571 Buoy 12 and d) BARC at Utqiaġvik in the 2015 Arctic Spring. Observations and error bars in red, BASE
572 BrO$_{LTcol}$ in brown, PACK BrO$_{LTcol}$ in purple, and BLOW+PACK BrO$_{LTcol}$ in orange. All BrO$_{LTcol}$ plotted
573 continuously except for gaps where dSCDO$_4$ >1*10^{43} molecules^{2}cm^{-5}.

574 **3.4 BLOW+PACK run best replicates hourly BrO events in mid and late May**

575   The model's hourly predictions of BrO$_{LTcol}$ in May 2015 are shown in Figure 6 for the BASE,

576 PACK, and BLOW+PACK runs. Figure 6 screens modeled BrO$_{LTcol}$ for times when dSCD O^4 >1*10^{43}

577 molecules^{2}cm^{-5}, while Supplemental Figures S7 and S8 make direct comparisons between observations of

578 BrO$_{LTcol}$ for O-Buoys (S7) and at Utqiaġvik (S8) throughout all of Spring 2015. The O-Buoys show

579 fluctuations in observed BrO$_{LTcol}$ during May and show consistent increased columns of BrO$_{LTcol}$ from

580 May 10 to May 20. The BASE run never rises above 10^{13} molecules/cm^2 and underpredicts most May

581 hourly BrO$_{LTcol}$, although it predicts monthly BrO$_{LTcol}$ on OB10 within observational errors in May and

582 June. Both PACK and BLOW+PACK runs show better skill in replicating BrO$_{LTcol}$. The addition of the

583 snowpack mechanism allows us to predict increased BrO$_{LTcol}$ in late May on O-Buoys 10 and 11. This

584   points to the role of surface snowpack in late-season events in agreement with the findings of Burd et al.

585   (2017).

586   We can identify the role of blowing snow SSA by comparing the PACK and BLOW+PACK runs.

587   Both PACK and BLOW+PACK runs underestimate BrO_{LTcol} during the first ten days of May. BrO

588   predictions and show higher variability and peaks starting on May 10. The blowing snow SSA

589   mechanism increases BLOW+PACK BrO_{LTcol} on May 12 and 13. PACK is skilled at replicating observed

590   O-Buoy 11 BrO_{LTcol} on both days, and both PACK and BLOW+PACK are within observational BrO_{LTcol}

591   error on May 13.

592   A BrO event also occurs on May 13 on O-Buoy 10. While the strength of the O-Buoy 10 BrO

593   event is overestimated by PACK and BLOW+PACK, the shape of that event is reproduced in both runs.

594   Observed BrO_{LTcol} decreases rapidly on all O-Buoys after May 14, and the model is unable to track this

595   sharp decrease. Rapid changes in BrO_{LTcol} may be caused by sharp edges in BrO-enriched airmasses such

596   as those seen by Simpson et al. (2017). GEOS-Chem run at this resolution cannot replicate abrupt

597   changes in BrO, but it does slowly decrease BrO_{LTcol} to reach BrO_{LTcol} to less than 10^{13} molecules/cm^2 on

598   May 16. The BLOW+PACK mechanism is skilled in replicating the magnitude and features of a mid-

599   May BrO event on O-Buoys 10 and 11.

600   Figure 7 shows all Spring 2015 BrO_{LTcol} observations on O-Buoys 10, 11, 12, and BARC plotted

601   against PACK BrO_{LTcol} and BLOW+PACK BrO_{LTcol}. The increase in BrO_{LTcol} on adding BLOW leads to

602   fewer underpredictions of observations (see bottom right section of Figure 7b). The Pearson correlation

603   coefficient (r) between PACK BrO_{LTcol} and observed BrO_{LTcol} is 0.33, improving to 0.39 on addition of

604   BLOW in the BLOW+PACK run. Other runs show less skill in replicating observations, with a BASE

605   BrO_{LTcol} Pearson correlation to observations of 0.19 and a BLOW BrO_{LTcol} Pearson correlation to

606   observations of 0.23. We also performed a simple linear regression to determine the relationship between

607   predictions and observations for each run. The slope of the line of best fit improves drastically on addition

608   of PACK, changing from 0.06 for BASE and 0.07 for BLOW to 0.33 for PACK and 0.44 for

609   BLOW+PACK. There is a positive synergistic effect on the slope of the line of best fit when using both

610   BLOW and PACK in combination rather than individually. The use of both BLOW and PACK

611   mechanisms corroborates literature findings on the processes influencing Arctic reactive bromine and

612   increases correlation between GEOS-Chem predictions and observations.

613
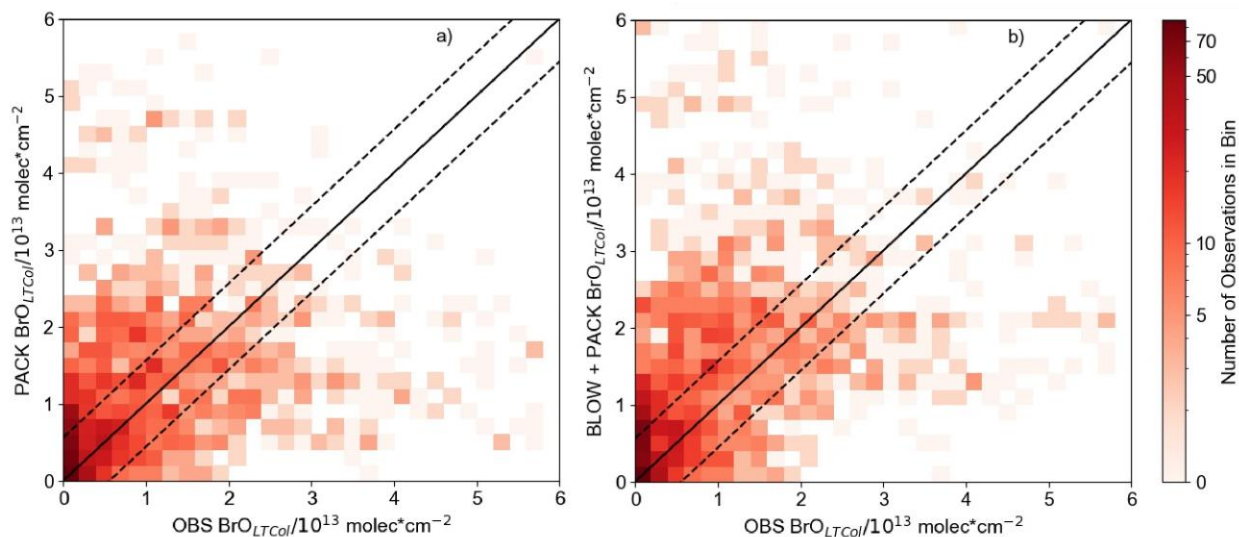
Figure 7: Hourly modeled BrO$_{LTcol}$ versus BrO$_{LTcol}$ observations

Two dimensional histograms showing density of GEOS-Chem predicted BrO$_{LTcol}$ versus all observed Spring 2015 hourly Br$_{LTcol}$, with a) PACK BrO$_{LTcol}$ shown at left sorted into square bins of 0.2 with an Pearson *r* correlation to observations of 0.33 and b) BLOW+PACK BrO$_{LTcol}$ on the bottom sorted into square bins of 0.2 with Pearson *r* correlation to observations to 0.39. All units are in molecules/cm^2. 1:1 line drawn in the center in black, with a margin of the average observational error plotted in dashed black lines around the central 1:1 line.

4. Arctic Spring reactive bromine modeling discussion

4.1 Use of both mechanisms in conjunction leads to best prediction of tropospheric BrO results

Initial implementation of this snowpack mechanism in Toyota et al. (2011) increased the daytime yield of Br$_2$ from ozone deposition to 7.5% to improve agreement between observed and modeled surface ozone mixing ratios. Toyota et al. (2011) also increased the surface resistance of ozone to 10^4 s/m, which decreased deposition velocities on Arctic snowpack to approximately 0.01 cm/s. Our model using a constant yield of Br$_2$ from ozone deposition at 0.1% performs best despite observations that sunlight has an effect on reactive bromine recycling in the snowpack (Pratt et al., 2013; Custard et al., 2017). GEOS-Chem does not explicitly model heterogeneous photochemistry within the snowpack interstitial space but does include heterogeneous bromine chemistry on aerosol particle surfaces after the Br$_2$ is emitted from the snowpack into the lowest model layer. The updates to GEOS-Chem halogen chemistry (Schmidt et al., 2016; Sherwen et al., 2016b; Chen et al., 2017; Wang et al., 2019b) should be mechanistically sufficient to model daytime heterogeneous chemistry of reactive bromine on aerosol surfaces. We note that improvements to GEOS-Chem have increased the explicit modeling of these photochemical recycling and amplification processes, possibly reducing the need for empirical increases to daytime yields.

Our findings differ from recent implementations of the snowpack mechanism in Herrmann et al. (2021) and Marelle et al. (2021). While all snowpack mechanisms are based on Toyota et al. (2011), several large differences in model configuration and mechanism implementation explain these

639   differences. We allow Br_2 production from ozone deposition over all snow surfaces, leading to much

640   higher Br_2 production over MYI and coastal regions. Land snowpack can produce Br_2 on exposure to

641   ozone and sunlight (Pratt et al., 2013; Custard et al., 2017) and Figure 4 shows our coastal snowpack

642   producing large quantities of Br_2. Tropospheric reactive bromine chemistry has been observed up to 200

643   km inland from the coast (Peterson et al., 2018). Marelle et al. (2021) underestimates BrO in late March

644   and overestimates Utqiaġvik BrO in early April. This seasonal pattern may be due to increased daytime

645   ozone yield on first year ice near Utqiaġvik in April. Herrmann et al. (2021) found that HOBr and $BrNO_3$

646   deposition was more important in driving snowpack Br_2 production and that the daytime yield of 7.5%

647   Br_2 on ozone deposition underpredicted BrO. We find that ozone contributes slightly more than HOBr

648   and $BrNO_3$ because we allow for Br_2 production on ozone deposition over multi-year ice and coastal

649   snowpack regions. The temporal coverage of this study spans the entire year, while Herrmann et al.

650   (2021) only spans February, March, and April. Our longer timescale highlights the issue of increased

651   daytime Br_2 yield during May and June (see Figure 4 PHOTOPACK) with increased emissions over the

652   Arctic Ocean that are not in agreement with satellite observations of minimal Arctic tropospheric BrO in

653   June (Richter et al., 1998).

4.2 Addition of PACK mechanism increases surface ozone predictive skill

655   The Barrow Arctic Research Center (BARC) in Utqiaġvik has the most comprehensive coverage

656   of surface ozone in Spring 2015. A constant yield of 0.1% Br_2 from ozone deposition allows us to

657   approximate the average vertical extent of ozone depletion events at Utqiaġvik in May 2015. The increase

658   in Br_y in the PACK and BLOW+PACK runs is confined to the lowest 1000 m of the atmosphere (see

659   Supplemental Figure S9). Ozone depletions, caused by reactive bromine chemistry, often only occur

660   within the lowest 1000 m of the troposphere (Bottenheim et al., 2002; Salawitch et al., 2010). Previous

661   studies have found evidence of lofted BrO in plumes at altitudes up to 900 m AGL (Peterson et al., 2017).

662   The monthly average Utqiaġvik May surface ozone in BLOW and BLOW+PACK is 22 nmol/mol,

663   matching mean May surface ozone from 1999-2008 (Oltmans et al., 2012). The PHOTOPACK runs

664   generate mean May surface ozone depletion to approximately 5 nmol/mol, far below the May mean. The

665   PACK and BLOW+PACK runs duplicate the approximate vertical extent of elevated bromine levels and

666   the strength of typical May ozone depletion.

667   Figure 8 shows hourly ozone predictions alongside BARC ozone observations (McClure-Begley,

668   Petropavlovskikh, and Oltmans, 2014). The BASE model fails to replicate variance in ozone measured at

669   BARC in Utqiaġvik, with a Pearson correlation coefficient to observations of 0.35. Adding PACK

670   improves Pearson correlation to 0.47, within rounding error of BLOW+PACK Pearson correlation of

671   0.47. Both PACK and BLOW+PACK significantly improve model performance in replicating ozone

672   depletions such as those below 30 nmol/mol from March 20 to March 29 but fail to track the subsequent

673   recovery of ozone to background levels on April 1. Predicted PACK ozone does not recover to

674   backgrounds levels up to the height of roughly 1000 m. A similar pattern where our model replicates low

675   ozone but fails to predict the recovery of ozone to background levels occurs on April 5 and 15.

676   Examination of ozone profiles in GEOS-Chem found that GEOS-Chem underpredicts tropospheric ozone

677   by 10-20 ppb north of 60° latitude (Wang et al., 2021), which contributes to the low ozone predictions in

678   our runs. Previous modeling of Utqiaġvik spring 2012 ozone in WRF-Chem found a similar linear

679   correlation coefficient of 0.5 to BROMEX observations (Simpson et al., 2017) when using both blowing

680   snow and snowpack mechanisms (Marelle et al., 2021). We are biased low compared to observations,

681   with a root mean square error of 17.0 nmol/mol in BLOW+PACK compared to a root mean square error

682   of 12.9 nmol/mol in Marelle et al. (2021). This may be partially due to limited vertical resolution in

683   GEOS-Chem that may be inadequate to describe shallow surface-based temperature inversions and

684   subsequent recovery. The high bias in ozone deposition velocity over sea ice surfaces may also contribute

685   to low ozone mixing ratios near the surface (Helmig et al., 2007).

686

687
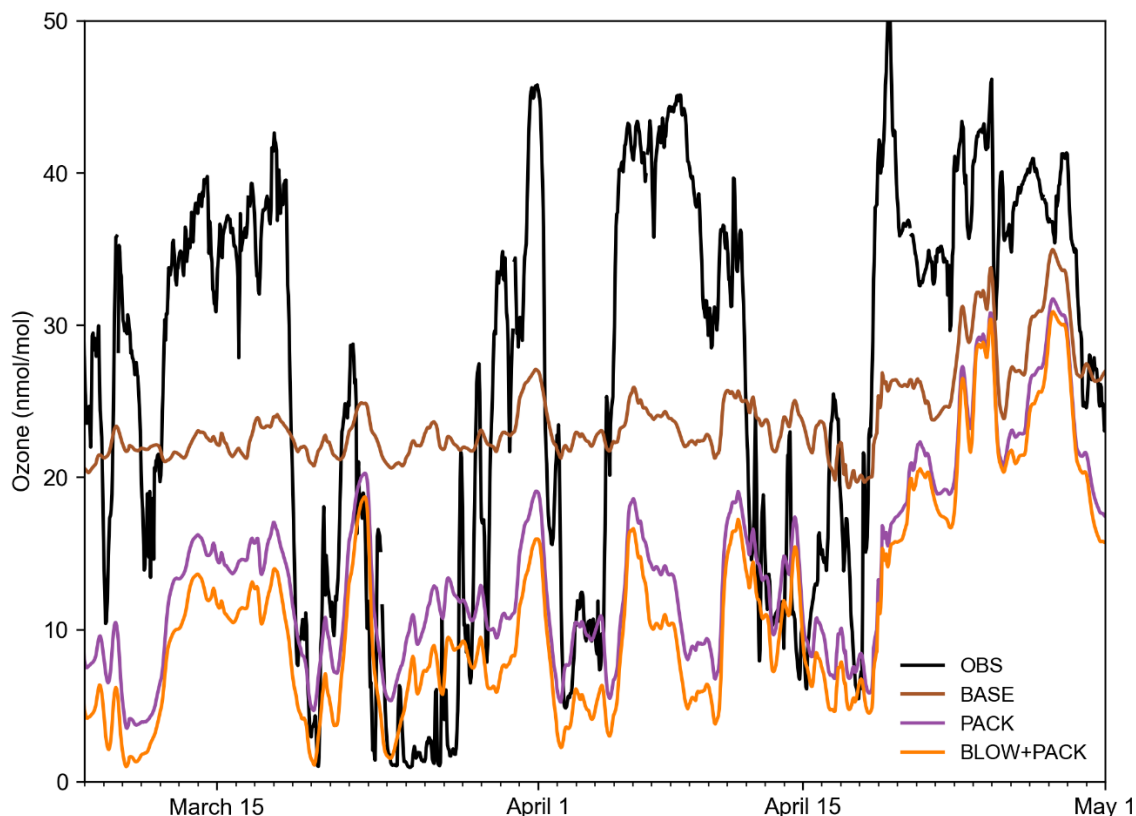
Figure 8: Hourly Utqiaġvik ozone timeseries
Hourly timeseries of BLOW+PACK, PACK, and BASE ozone at Utqiaġvik in the 2015 Arctic Spring.
Ozone observations at BARC in black (McClure-Begley, Petropavlovskikh and Oltmans, 2014), BASE
ozone in brown, PACK ozone in purple, and BLOW+PACK ozone in orange. Gaps indicate missing
observational data.

A similar improvement in ozone predictions on the addition of PACK is seen on the O-Buoys, but

is harder to quantify due to observational gaps in ozone data. Supplemental Figure S10 shows hourly

ozone predictions graphed over O-Buoy 11 observations and Supplemental Figure S11 shows hourly

ozone predictions graphed over O-Buoy 12. O-Buoy 10 was not able to gather an observations of ozone in

2015. The clearest impact of PACK in Figures S10 and S11 is seen in early April, with observed ozone

dropping near zero nmol/mol and PACK and BLOW+PACK runs dropping to five nmol/mol while the

BASE run remains near 20 nmol/mol. Figure S10 shows that ozone predictions on O-Buoy 10 in May are

less accurate, failing to fall below 10 nmol/mol ozone while observations show ozone dropping near the

detection limit. The O-Buoys appear to experience more late-season ozone depletion events that GEOS-

Chem fails to replicate, possibly due to warming temperatures increasing vertical mixing and replenishing

ozone near the surface.

705

Table 3: Arctic Tropospheric Reactions Rates by Model Run

Rates for each of the simulated reactions listed in Figure 1 grouped by GEOS-Chem run. All units are listed as millions of moles per hour across the region shown in Supplemental Figure S14. R in equation R2 refers to any organic molecule. Y in equation 1 represents NO, Cl, or H. X in equation HR6a represents either Br or Cl. PHOTOPACK and BLOW+PHOTOPACK are excluded as they severely overpredict BrO as seen in Figures 4 and 5.

	BASE	BLOW	PACK	BLOW+PACK	Reaction Equation
R1	17.57	17.77	27.7	28.4	$BrO + YO \rightarrow Br + O_2$
R2	236.28	261.75	435.74	472.14	$Br + O_3 \rightarrow BrO + O_2$
R3	0.7	0.84	1.38	1.54	$Br + RH \rightarrow HBr, Br + HO_2 \rightarrow HBr$
R4	0.01	0.01	0.02	0.02	$HBr + OH \rightarrow Br + H_2O$
R5	9.41	9.47	14.41	14.01	$BrO + HO_2 \rightarrow HOBr$
R6	1.63	2.4	12.78	16.16	$BrO + BrO \rightarrow Br_2 + O_2$
R7	0.03	0.06	0.04	0.06	$BrO + ClO \rightarrow BrCl + O_2$
R8	2.8	2.94	5.69	5.86	$BrO + NO_2 \rightarrow BrNO_3$
R9	0	0	0	0	$Br_2 + OH \rightarrow Br + HOBr$
R10	0.15	0.17	1.39	1.64	$Br + BrNO_3 \rightarrow Br_2 + NO_3$
R11	0.18	0.18	0.55	0.7	$Br + NO_2 \rightarrow BrNO_2$
HR1a	0.04	0.03	0.15	0.1	$HOBr + HBr \rightarrow Br_2 + H_2O$
HR1b	0.79	0.95	1.47	1.68	$HOBr + p\text{-}Br^- \rightarrow Br_2 + OH^-$
HR2	0.17	0.21	0.38	0.38	$HOBr + H_2O + HSO_3^- \rightarrow H_2SO_4 + HBr + OH^-$
HR3	0.25	0.29	0.43	0.44	$BrNO_3 + H_2O \rightarrow HNO_3 + HOBr$
HR4a	0	0	0	0	$HBr + O_3 \rightarrow HOBr + O_2$
HR4b	0.07	0.09	0.14	0.15	$p\text{-}Br^- + O_3 + H_2O \rightarrow HOBr + O_2 + OH^-$
HR5	0	0	0	0	$BrNO_3 + HCl \rightarrow BrCl + HNO_3$
HR6a	0	0	0	0	$HOX + HX \rightarrow BrCl + H_2O$
HR6b	0.29	0.54	0.37	0.68	$HOBr + p\text{-}Cl^- \rightarrow BrCl + OH^-$
HR7a	0	0	0	0	$HBr + ClNO_x \rightarrow BrCl + HNO_x$
HR7b	0	0	0	0	$p\text{-}Br^- + ClNO_x + H_2O \rightarrow BrCl + HNO_x + OH^-$
HR8	0	0	0	0	$p\text{-}Br^- + IO_x > IBr + O_x$
P1	1.38	1.76	6.04	7.24	$Br_2 + hv \rightarrow 2Br$
P2	203.54	227.07	362.89	392.04	$BrO + hv \rightarrow Br + O$
P3	8.45	8.11	12.6	11.75	$HOBr + hv \rightarrow OH + Br$
P4	0.36	0.37	0.57	0.56	$BrNO_3 + hv \rightarrow BrO + NO_2$
P5	2.04	2.1	3.24	3.17	$BrNO_3 + hv \rightarrow Br + NO_3$
P6	0.18	0.18	0.55	0.7	$BrNO_2 + hv \rightarrow Br + NO_2$
P7	0.35	0.63	0.45	0.76	$BrCl + hv \rightarrow Br + Cl$
P8	0	0	0	0	$BrI + hv \rightarrow Br + I$

5. Examining reactive bromine in the Arctic in September and October

O-Buoys deployed during fall 2015 measured BrO slant column densities characterized by noise around zero (see Supplemental Figures S12 and S13). We do not retrieve vertical column density from these fall slant column densities, because the resulting retrievals would be biased positive due to an algorithm requirement that only positive BrO column densities are allowed in the optimal estimation inversion. These differential slant column densities (dSCDs) can be used qualitatively to determine the presence or absence of BrO above the detection limit. If the dSCDs display noise around zero at all viewing angles, the BrO in the troposphere is below the detection limit of the spectrometer. A pattern of larger BrO dSCDs at near-horizon viewing elevation angles indicating the presence of tropospheric BrO above the detection limit is only observed at Utqiaġvik during Arctic Spring (see Supplemental Figure S12) . Any BrO present in the Arctic troposphere in September and October falls below detection limits at Utqiaġvik (see Supplemental Figure S12) and on each O-Buoy (see Supplemental Figure S13). The average Arctic Spring 2015 MAX-DOAS BrO_{LTcol} detection limits are 5 x 10^{12} molecules/cm^2 (Peterson et al., 2015; Simpson et al., 2017; Swanson et al., 2020). Both BLOW and PACK mechanisms lead to prediction of increased fall BrO because the weather and sea ice conditions specified in the emission algorithms occur in fall as well as spring.

Figure 9 shows fall predictions of BrO_{LTcol} filtered for times when solar elevation angle was greater than 5˚. BASE and PACK BrO_{LTcol} remain near zero in September but rise above the MAX-DOAS detection limit of 5 x10^{12} molecules/cm^2 BrO_{LTcol} in October. The addition of the blowing snow SSA mechanism propels BLOW BrO_{LTcol} up to 6 x 10^{13} molecules/cm^2 in October. O-Buoys 13 and 14 have the highest modeled fall BrO_{LTcol} but even Utqiaġvik has several days of BrO_{LTcol} above 5 x10^{12} molecules/cm^2 in late October. There is no clear evidence of any BrO above MAX-DOAS detection limits at Utqiaġvik or on any O-Buoy in October, as seen by the dSCDs scattered around zero in Supplemental Figures S12 and S13.

738
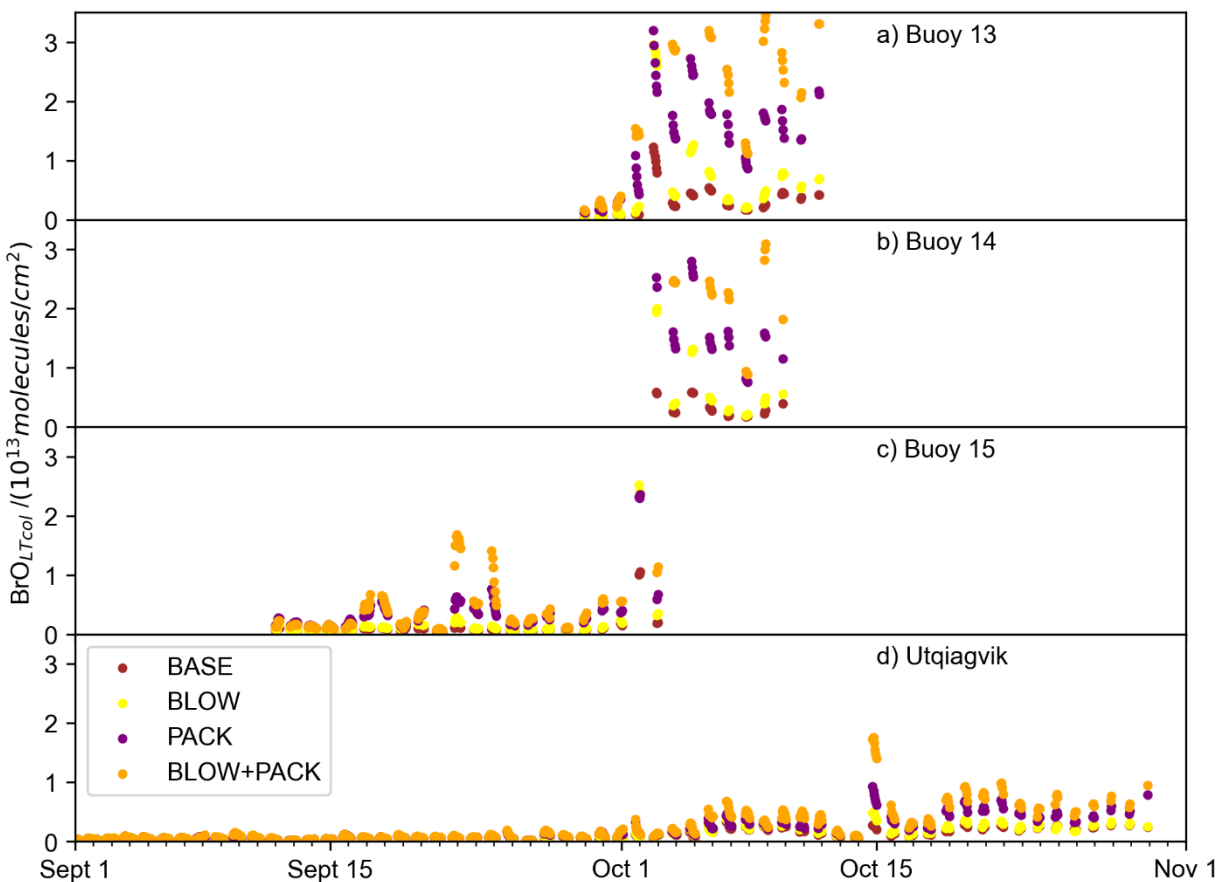
Figure 9: Fall GEOS-Chem Predicted BrO$_{LTcol}$
Hourly timeseries of BLOW+PACK, PACK, and BASE BrO$_{LTcol}$ on a) O-Buoy 10, b) O-Buoy 11, c) O-Buoy 12 and d) BARC at Utqiaġvik during September and October 2015 BASE BrO$_{LTcol}$ in brown, BLOW BrO$_{LTcol}$ in yellow, PACK BrO$_{LTcol}$ in purple, and BLOW+PACK BrO$_{LTcol}$ in orange. All BrO$_{LTcol}$ plotted continuously except for gaps where solar elevation angle was less than 5˚.

Both mechanisms assume that snowpack and SSA are just as capable of recycling reactive bromine as in the springtime. High fall and winter SSA agrees with observations of peak SSA during polar winter in both Antarctica (Wagenbach et al., 1998) and in the Arctic (Jacobi et al., 2012). The deposition of Arctic haze (Douglas and Sturm, 2004) and SSA (Jacobi et al., 2019) increases snowpack salinity and sulfate content over the course of winter and spring. This seasonal change in snowpack salinity and acidity may enable reactive bromine recycling in the Arctic Spring, but there may not be sufficient haze and SSA deposition in fall to decrease snowpack pH and increase snowpack bromide content. Additional observations of fall snowpack over sea ice including ion content could show different snowpack composition in spring and fall. Thus, the GEOS-Chem model overestimates fall BrO by assuming the fall snowpack is equally capable of reactive bromine recycling as spring snowpack and providing an infinite reservoir of snowpack bromide in all seasons. Most other modeling exercises have

756 focused on spring with unknown predictions in fall, possibly indicating problems in mechanisms or
757 parameterizations being employed, so we suggest that modeling should be done for a full year to improve
758 underlying chemistry and physics. We also suggest a fall snow sampling campaign to validate modeled
759 fall BrO.

6. Conclusions

761   We add snowpack Br_2 production to GEOS-Chem based on multiple field observations
762 demonstrating molecular bromine production in snowpack interstitial air. We use a mechanistic
763 parameterization of snowpack Br_2 production based on Toyota et al. (2011) in which Br_2 is emitted from
764 all snowpack of sufficient salinity and depth over land and sea ice upon deposition of the precursor
765 species HOBr, $BrNO_3$, and ozone. Prior work has also added a blowing snow SSA production mechanism
766 that increases aerosol particulate bromide and thus facilitates heterogeneous recycling of reactive bromine
767 on these aerosol particle surfaces. We update the halogen scheme to GEOS-Chem 12.9.3 and performed
768 six model simulations including a BASE run with neither blowing snow SSA nor snowpack emissions, a
769 PACK run assuming constant yield of Br_2 on ozone deposition over all snow surfaces, a PHOTOPACK
770 run assuming increased daytime yield of Br_2 on ozone deposition (similar in Toyota et al., 2011), a
771 BLOW run using only blowing snow SSA formation and two additional runs combing BLOW and each
772 respective PACK mechanism. The increased daytime yield of Br_2 in PHOTOPACK leads to
773 overprediction of BrO in these simulations, but the PACK run (with constant Br_2 yield day and night)
774 matches monthly averaged BrO vertical column densities within measurement error for 9 of 13 cases at
775 O-Buoy and Utqiagvik in springtime months. The PACK and BLOW+PACK runs were successful in
776 replicating observed BrO events on O-Buoys in May. The BLOW mechanism effectively increases
777 aerosol surface available for turnover of reactive bromine. The snowpack mechanism has more impact on
778 modeled BrO mixing ratios than the blowing snow SSA mechanism, but both contribute to tropospheric
779 reactive bromine. We extend our model run to the full year and find that enhanced daytime Br_2 yield can
780 lead to increased Arctic Ocean Br_2 production in the summer. Examining modeled BrO in fall 2015
781 reveals prediction of BrO when using these mechanisms that are at odds with observations.

782   The inclusion of two Arctic reactive bromine production mechanisms based on literature
783 observations of snowpack Br_2 emission and blowing snow SSA formation improves model skill in
784 replicating Arctic tropospheric BrO in spring 2015. The snowpack is an important source of reactive
785 bromine, and SSA particles provide an abundant surface for sustained reactive bromine recycling in the
786 troposphere. We find that using both snowpack and blowing snow SSA bromine production mechanisms
787 is necessary for modeling BrO in the Arctic.

788

789 *Competing interests:* The authors declare that they have no conflict of interest.

790 Author contributions. WFS, WRS and CH designed the study. WRS collected and curated MAX-DOAS

791 data. KC, LM, JT, LJ, JH and contributed code for reactive bromine mechanisms. CH, KC, LJ, JH, BA,

792 SZ, QC, XW, and TS contributed model updates. WFS carried out modeling and analysis. WFS wrote the

793 paper with input from all authors.

7. Acknowledgements

795 We acknowledge support from the National Science Foundation for providing funding under grants ARC-

796 1602716, AGS-1702266, AGS-2109323, and ARC-1602883. This work also supported by the CNRS

797 INSU LEFE-CHAT program under the grant Brom-Arc, and NASA grant 80NSSC19K1273. This

798 research has received funding from the European Union's Horizon 2020 research and innovation program

799 under grant agreement no. 689443 via project iCUPE (Integrative and Comprehensive Understanding on

800 Polar Environments). The O-Buoy and Utqiagvik ground-based BrO datasets are available in the

801 arcticdata.io repository (doi:10.18739/A2WD4W). We recognize the work of Jiayue Huang in adding the

802 blowing snow SSA mechanism to GEOS-Chem. We would like to thank the National Oceanic and

803 Atmospheric Administration (NOAA) Global Monitoring Division for the provision of ozone and

804 temperature data near Utqiaġvik available online at doi:10.7289/V57P8WBF. We acknowledge use of the

805 coastline distance dataset from the Pacific Islands Ocean Observing System. We acknowledge the use of

806 imagery from the Land Atmosphere Near Real-Time Capability for EOS (LANCE) system and services

807 from the Global Imagery Browse Services (GIBS), both operated by the NASA/GSFC/Earth Science Data

808 and Information System (ESDIS, https://earthdata.nasa.gov) with funding provided by NASA/HQ. We

809 owe a debt of gratitude to all members of the Atmospheric Chemistry and Global Change group at Florida

810 State University for their support for working with GEOS-Chem and Python. We thank the global GEOS-

811 Chem community for their tireless work to improve the model. We also thank all involved in the O-Buoy

812 project for data collection and analysis.

8. References

814 Alexander, B., Park, R. J., Jacob, D. J., Li, Q. B., Yantosca, R. M., Savarino, J., Lee, C. C. W. and
815 Thiemens, M. H.: Sulfate formation in sea-salt aerosols: Constraints from oxygen isotopes, J. Geophys.
816 Res. D Atmos., 110(10), 1–12, doi:10.1029/2004JD005659, 2005.

817 AMAP: Arctic Monitoring and Assessment Program 2011: Mercury in the Arctic., 2011.

818 Artiglia, L., Edebeli, J., Orlando, F., Chen, S., Lee, M. T., Corral Arroyo, P., Gilgen, A., Bartels-Rausch,
819 T., Kleibert, A., Vazdar, M., Andres Carignano, M., Francisco, J. S., Shepson, P. B., Gladich, I. and
820 Ammann, M.: A surface-stabilized ozonide triggers bromide oxidation at the aqueous solution-vapour
821 interface, Nat. Commun., 8(1), 1–7, doi:10.1038/s41467-017-00823-x, 2017.

822 Ayers, G. P., Gillett, R. W., Cainey, J. M. and Dick, A. L.: Chloride and bromide loss from sea-salt

823   particles in Southern Ocean air, J. Atmos. Chem., 33(3), 299–319, doi:10.1023/A:1006120205159, 1999.

824   Bariteau, L., Helmig, D., Fairall, C. W., Hare, J. E., Hueber, J. and Lang, E. K.: Determination of oceanic
825   ozone deposition by ship-borne eddy covariance flux measurements, Atmos. Meas. Tech., 3(2), 441–455,
826   doi:10.5194/amt-3-441-2010, 2010.

827   Barrie, L. A., Bottenheim, J. W., Schnell, R. C., Crutzen, P. J. and Rasmussen, R. A.: Ozone destruction
828   and photochemical reactions at polar sunrise in the lower Arctic atmosphere, Nature, 334(6178), 138–
829   141, doi:10.1038/334138a0, 1988.

830   Berg, W. W., Sperry, P. D., Rahn, K. A. and Gladney, E. S.: Atmospheric Bromine in the Arctic, J.
831   Geophys. Res., 88(3), 6719–6736, doi:10.1029/JC088iC11p06719, 1983.

832   Bey, I., Jacob, D. J., Yantosca, R. M., Logan, J. A., Field, B. D., Fiore, A. M., Li, Q., Liu, H. Y., Mickley,
833   L. J. and Schultz, M. G.: Global modeling of tropospheric chemistry with assimilated meteorology:
834   Model description and evaluation, J. Geophys. Res. Atmos., 106(D19), 23073–23095,
835   doi:10.1029/2001JD000807, 2001.

836   Bottenheim, J. W., Fuentes, J. D., Tarasick, D. W. and Anlauf, K. G.: Ozone in the Arctic lower
837   troposphere during winter and spring 2000 (ALERT2000), Atmos. Environ., 36, 2535–2544, 2002.

838   Burd, J. A., Peterson, P. K., Nghiem, S. V., Perovich, D. K. and Simpson, W. R.: Snow Melt Onset
839   Hinders Bromine Monoxide Heterogeneous Recycling in the Arctic, J. Geophys. Res. Atmos., 1–13,
840   doi:10.1002/2017JD026906, 2017.

841   Cao, L., Platt, U. and Gutheil, E.: Role of the boundary layer in the occurrence and termination of the
842   tropospheric ozone depletion events in polar spring, Atmos. Environ., 132, 98–110,
843   doi:10.1016/j.atmosenv.2016.02.034, 2016.

844   Carlson, D., Donohoue, D., Platt, U. and Simpson, W. R.: A low power automated MAX-DOAS
845   instrument for the Arctic and other remote unmanned locations, Atmos. Meas. Tech., 429–439, 2010.

846   Chance, K.: Analysis of BrO Measurements from the Global Ozone Monitoring Experiment, Geophys.
847   Res. Lett., 25(17), 3335–3338, 1998.

848   Chen, Q., Schmidt, J. A., Shah, V., Jaeglé, L., Sherwen, T. and Alexander, B.: Sulfate production by
849   reactive bromine: Implications for the global sulfur and reactive bromine budgets, Geophys. Res. Lett.,
850   44(13), 7069–7078, doi:10.1002/2017GL073812, 2017.

851   Choi, S., Wang, Y., Salawitch, R. J., Canty, T., Joiner, J., Zeng, T., Kurosu, T. P., Chance, K., Richter,
852   A., Huey, L. G., Liao, J., Neuman, J. A., Nowak, J. B., Dibb, J. E., Weinheimer, A. J., Diskin, G.,
853   Ryerson, T. B., Da Silva, A., Curry, J., Kinnison, D., Tilmes, S. and Levelt, P. F.: Analysis of satellite-
854   derived Arctic tropospheric BrO columns in conjunction with aircraft measurements during ARCTAS and
855   ARCPAC, Atmos. Chem. Phys., 12(3), 1255–1285, doi:10.5194/acp-12-1255-2012, 2012.

856   von Clarmann, T. and Glatthor, N.: The application of mean averaging kernels to mean trace gas
857   distributions, Atmos. Meas. Tech. Discuss., 1–11, doi:10.5194/amt-2019-61, 2019.

858   Clemer, K., Van Roozendael, M., Fayt, C., Hendrick, F., Hermans, C., Pinardi, G., Spurr, R., Wang, P.
859   and Maziere, M. De: Multiple wavelength retrieval of tropospheric aerosol optical properties from
860   MAXDOAS measurements in Beijing, Atmos. Meas. Tech., 3, 863–878, doi:10.5194/amt-3-863-2010,
861   2010.

862   Custard, K. D., Raso, A. R. W., Shepson, P. B., Staebler, R. M. and Pratt, K. A.: Production and Release
863   of Molecular Bromine and Chlorine from the Arctic Coastal Snowpack, ACS Earth Sp. Chem., 1, 142–
864   151, doi:10.1021/acsearthspacechem.7b00014, 2017.

Dery, S. J. and Yau, M. K.: A Bulk Blowing Snow Model, Bound. Layer Meteorol., 93, 237–251, 1999.

Déry, S. J. and Yau, M. K.: Simulation of blowing snow in the Canadian Arctic using a double-moment model, Boundary-Layer Meteorol., 99(2), 297–316, doi:10.1023/A:1018965008049, 2001.

Domine, F., Sparapani, R., Ianniello, A. and Beine, H. J.: The origin of sea salt in snow on Arctic sea ice and in coastal regions, Atmos. Chem. Phys. Discuss., 4(4), 4737–4776, doi:10.5194/acpd-4-4737-2004, 2004.

Douglas, T. A. and Sturm, M.: Arctic haze, mercury and the chemical composition of snow across northwestern Alaska, Atmos. Environ., doi:10.1016/j.atmosenv.2003.10.042, 2004.

Eastham, S. D., Weisenstein, D. K. and Barrett, S. R. H.: Development and evaluation of the unified tropospheric-stratospheric chemistry extension (UCX) for the global chemistry-transport model GEOS-Chem, Atmos. Environ., 89, 52–63, doi:10.1016/j.atmosenv.2014.02.001, 2014.

Falk, S. and Sinnhuber, B. M.: Polar boundary layer bromine explosion and ozone depletion events in the chemistry-climate model EMAC v2.52: Implementation and evaluation of AirSnow algorithm, Geosci. Model Dev., 11(3), 1115–1131, doi:10.5194/gmd-11-1115-2018, 2018.

Fan, S. M. and Jacob, D. J.: Surface ozone depletion in Arctic spring sustained by bromine reactions on aerosols, Nature, 359(6395), 522–524, doi:10.1038/359522a0, 1992.

Fischer, E. V., Jacob, D. J., Yantosca, R. M., Sulprizio, M. P., Millet, D. B., Mao, J., Paulot, F., Singh, H. B., Roiger, A., Ries, L., Talbot, R. W., Dzepina, K. and Pandey Deolal, S.: Atmospheric peroxyacetyl nitrate (PAN): A global budget and source attribution, Atmos. Chem. Phys., 14(5), 2679–2698, doi:10.5194/acp-14-2679-2014, 2014.

Fisher, J. A., Jacob, D. J., Travis, K. R., Kim, P. S., Marais, E. A., Miller, C. C., Yu, K., Zhu, L., Yantosca, R. M., Sulprizio, M. P., Mao, J., Wennberg, P. O., Crounse, J. D., Teng, A. P., Nguyen, T. B., Clair, J. M. S., Cohen, R. C., Romer, P., Nault, B. A., Wooldridge, P. J., Jimenez, J. L., Campuzano-Jost, P., Day, D. A., Hu, W., Shepson, P. B., Xiong, F., Blake, D. R., Goldstein, A. H., Misztal, P. K., Hanisco, T. F., Wolfe, G. M., Ryerson, T. B., Wisthaler, A. and Mikoviny, T.: Organic nitrate chemistry and its implications for nitrogen budgets in an isoprene- and monoterpene-rich atmosphere: Constraints from aircraft (SEAC4RS) and ground-based (SOAS) observations in the Southeast US, Atmos. Chem. Phys., 16(9), 5969–5991, doi:10.5194/acp-16-5969-2016, 2016.

Foster, K. L., Plastridge, R. A., Bottenheim, J. W., Shepson, P. B., Finlayson-pitts, B. J. and Spicer, C. W.: The Role of Br 2 and BrCl in Surface Ozone Destruction at Polar Sunrise, Science (80-.)., 291(JANUARY), 471–475, 2001.

Frey, M. M., Norris, S. J., Brooks, I. M., Anderson, P. S., Nishimura, K., Yang, X., Jones, A. E., Nerentorp Mastromonaco, M. G., Jones, D. H. and Wolff, E. W.: First direct observation of sea salt aerosol production from blowing snow above sea ice, Atmos. Chem. Phys., (April), 1–53, doi:10.5194/acp-2019-259, 2020.

Frieß, U., Monks, P. S., Remedios, J. J., Rozanov, A., Sinreich, R., Wagner, T. and Platt, U.: MAX-DOAS O4 measurements: A new technique to derive information on atmospheric aerosols: 2. Modeling studies, J. Geophys. Res, 111, 20, doi:10.1029/2005JD006618, 2006.

Frieß, U., Beirle, S., Bonilla, L. A., Bösch, T., Friedrich, M. M., Hendrick, F., Piters, A., Richter, A., Roozendael, M. Van, Rozanov, V. V, Spinei, E. and Tirpitz, J.: Intercomparison of MAX-DOAS vertical profile retrieval algorithms : studies using synthetic data, Atmos. Meas. Tech., (2), 2155–2181, 2019.

Gelaro, R., McCarty, W., Suarez, M. J., Todling, R., Molod, A., Takacs, L., Randles, C., Darmenov, A., Bosilovich, M., Reichle, R., Wargan, K., Coy, L., Cullather, R., Draper, C., Akella, S., Buchard, V.,

908 Conaty, A., Da Silva, A., Gu, W., Kim, G., Koster, R., Lucchesi, R., Merkova, D., Nielsen, J. E., Partyka,
909 G., Pawson, S., Putman, W., Rienecker, M., Schubert, S., Sienkiewicz, M. and Zhao, B.: The Modern-Era
910 Retrospective Analysis for Research and Applications , J. Clim., 30, 5419–5454, doi:10.1175/JCLI-D-16-
911 0758.1, 2017.

912 Group, N. O. B. P. and Stumpf, R.: Distance to Nearest Coastline: 0.01 Degree Grid, [online] Available
913 from: https://pae-paha.pacioos.hawaii.edu/thredds/ncss/dist2coast_1deg/dataset.html, 2021.

914 Halfacre, J. W., Knepp, T. N., Shepson, P. B., Thompson, C. R., Pratt, K. A., Li, B., Peterson, P. K.,
915 Walsh, S. J., Simpson, W. R., Matrai, P. A., Bottenheim, J. W., Netcheva, S., Perovich, D. K. and Richter,
916 A.: Temporal and spatial characteristics of ozone depletion events from measurements in the Arctic,
917 Atmos. Chem. Phys., 14(10), 4875–4894, doi:10.5194/acp-14-4875-2014, 2014.

918 Halfacre, J. W., Shepson, P. B. and Pratt, K. A.: pH-dependent production of molecular chlorine,
919 bromine, and iodine from frozen saline surfaces, Atmos. Chem. Phys, 19, 4917–4931, 2019.

920 Hara, K., Osada, K., Yabuki, M., Takashima, H., Theys, N. and Yamanouchi, T.: Important contributions
921 of sea-salt aerosols to atmospheric bromine cycle in the Antarctic coasts, Sci. Rep., 8(1),
922 doi:10.1038/s41598-018-32287-4, 2018.

923 Helmig, D., Ganzeveld, L., Butler, T. and Oltmans, S. J.: The role of ozone atmosphere-snow gas
924 exchange on polar, boundary-layer tropospheric ozone - A review and sensitivity analysis, Atmos. Chem.
925 Phys., 7(1), 15–30, doi:10.5194/acp-7-15-2007, 2007.

926 Herrmann, M., Sihler, H., Frieß, U., Wagner, T., Platt, U. and Gutheil, E.: Time-dependent 3D
927 simulations of tropospheric ozone depletion events in the Arctic spring using the Weather Research and
928 Forecasting model coupled with Chemistry (WRF-Chem), 7611–7638, 2021.

929 Holmes, C. D., Jacob, D. J., Corbitt, E. S., Mao, J., Yang, X., Talbot, R. and Slemr, F.: Global
930 atmospheric model for mercury including oxidation by bromine atoms, Atmos. Chem. Phys., 10(24),
931 12037–12057, doi:10.5194/acp-10-12037-2010, 2010.

932 Hönninger, G. and Platt, U.: Observations of BrO and its vertical distribution during surface ozone
933 depletion at Alert, Atmos. Environ., 36(15–16), 2481–2489, doi:10.1016/S1352-2310(02)00104-8, 2002.

934 Hönninger, G., von Friedeburg, C. and Platt, U.: Multi Axis Differential Optical Absorption Spectroscopy
935 (MAX-DOAS), Atmos. Chem. Phys., 4, 231–254, doi:10.5194/acpd-3-5595-2003, 2004.

936 Huang, J. and Jaeglé, L.: Wintertime enhancements of sea salt aerosol in polar regions consistent with a
937 sea-ice source from blowing snow, Atmos. Chem. Phys., (November), 1–23, doi:10.5194/acp-2016-972,
938 2017.

939 Huang, J., Jaeglé, L. and Shah, V.: Using CALIOP to constrain blowing snow emissions of sea salt
940 aerosols over Arctic and Antarctic sea ice, Atmos. Chem. Phys., 16253–16269, 2018.

941 Huang, J., Jaeglé, L., Chen, Q., Alexander, B., Sherwen, T., Evans, M., Theys, N. and Choi, S.:
942 Evaluating the impact of blowing snow sea salt aerosol on springtime BrO and O3 in the Arctic, Atmos.
943 Chem. Phys., 1–36, doi:10.5194/acp-2019-1094, 2020.

944 Jacobi, H. W., Voisin, D., Jaffrezo, J. L., Cozic, J. and Douglas, T. A.: Chemical composition of the
945 snowpack during the OASIS spring campaign 2009 at Barrow, Alaska, J. Geophys. Res. Atmos.,
946 doi:10.1029/2011JD016654, 2012.

947 Jacobi, H. W., Obleitner, F., Da Costa, S., Ginot, P., Eleftheriadis, K., Aas, W. and Zanatta, M.:
948 Deposition of ionic species and black carbon to the Arctic snowpack: Combining snow pit observations
949 with modeling, Atmos. Chem. Phys., 19(15), 10361–10377, doi:10.5194/acp-19-10361-2019, 2019.

Jaeglé, L., Quinn, P. K., Bates, T. S., Alexander, B. and Lin, J. T.: Global distribution of sea salt aerosols: New constraints from in situ and remote sensing observations, Atmos. Chem. Phys., 11(7), 3137–3157, doi:10.5194/acp-11-3137-2011, 2011.

Keller, C. A., Long, M. S., Yantosca, R. M., Da Silva, A. M., Pawson, S. and Jacob, D. J.: HEMCO v1.0: A versatile, ESMF-compliant component for calculating emissions in atmospheric models, Geosci. Model Dev., 7(4), 1409–1417, doi:10.5194/gmd-7-1409-2014, 2014.

Knepp, T. N., Bottenheim, J., Carlsen, M., Carlson, D., Donohoue, D., Friederich, G., Matrai, P. A., Netcheva, S., Perovich, D. K., Santini, R., Shepson, P. B., Simpson, W., Valentic, T., Williams, C. and Wyss, P. J.: Development of an autonomous sea ice tethered buoy for the study of ocean-atmosphere-sea ice-snow pack interactions: The O-buoy, Atmos. Meas. Tech., 3(1), 249–261, doi:10.5194/amt-3-249-2010, 2010.

Koo, J. H., Wang, Y., Kurosu, T. P., Chance, K., Rozanov, A., Richter, A., Oltmans, S. J., Thompson, A. M., Hair, J. W., Fenn, M. A., Weinheimer, A. J., Ryerson, T. B., Solberg, S., Huey, L. G., Liao, J., Dibb, J. E., Neuman, J. A., Nowak, J. B., Pierce, R. B., Natarajan, M. and Al-Saadi, J.: Characteristics of tropospheric ozone depletion events in the Arctic spring: Analysis of the ARCTAS, ARCPAC, and ARCIONS measurements and satellite BrO observations, Atmos. Chem. Phys., 12(20), 9909–9922, doi:10.5194/acp-12-9909-2012, 2012.

Krnavek, L., Simpson, W. R., Carlson, D., Domine, F., Douglas, T. A. and Sturm, M.: The chemical composition of surface snow in the Arctic: Examining marine, terrestrial, and atmospheric influences, Atmos. Environ., 50, 349–359, doi:10.1016/j.atmosenv.2011.11.033, 2012.

De Leeuw, G., Andreas, E. L., Anguelova, M. D., Fairall, C. W., Lewis, E. R., O'Dowd, C., Schulz, M. and Schwartz, S. E.: Production flux of sea spray aerosol, Rev. Geophys., 49(2), 1–39, doi:10.1029/2010RG000349, 2011.

Lehrer, E., Hönninger, G. and Platt, U.: A one dimensional model study of the mechanism of halogen liberation and vertical transport in the polar troposphere, Atmos. Chem. Phys., 4(11/12), 2427–2440, doi:10.5194/acp-4-2427-2004, 2004.

Lewis, E. R. and Schwartz, S. E.: Salt Aerosol Production: Mechanisms, Methods, Measurements, and Models: A Critical Review, American Geophysical Union, Washington D.C., 2004.

Lin, H., Jacob, D. J., Lundgren, E. W., Sulprizio, M. P., Keller, C. A., Fritz, T. M., Eastham, S. D., Emmons, L. K., Campbell, P. C., Baker, B., Saylor, R. D. and Montuoro, R.: Harmonized Emissions Component (HEMCO) 3.0 as a versatile emissions component for atmospheric models: Application in the GEOS-Chem, NASA GEOS, WRF-GC, CESM2, NOAA GEFS-Aerosol, and NOAA UFS models, Geosci. Model Dev., 14(9), 5487–5506, doi:10.5194/gmd-14-5487-2021, 2021.

Liu, T., Chan, A. W. H. and Abbatt, J. P. D.: Multiphase Oxidation of Sulfur Dioxide in Aerosol Particles: Implications for Sulfate Formation in Polluted Environments, Environ. Sci. Technol., acs.est.0c06496, doi:10.1021/acs.est.0c06496, 2021.

Mao, J., Paulot, F., Jacob, D. J., Cohen, R. C., Crounse, J. D., Wennberg, P. O., Keller, C. A., Hudman, R. C., Barkley, M. P. and Horowitz, L. W.: Ozone and organic nitrates over the eastern United States: Sensitivity to isoprene chemistry, J. Geophys. Res. Atmos., 118(19), 11256–11268, doi:10.1002/jgrd.50817, 2013.

Marelle, L., Thomas, J. L., Ahmed, S., Tuite, K., Stutz, J., Dommergue, A., Simpson, W. R., Frey, M. M. and Baladima, F.: Implementation and Impacts of Surface and Blowing Snow Sources of Arctic Bromine Activation Within WRF-Chem 4.1.1, J. Adv. Model. Earth Syst., 13(8), doi:10.1029/2020ms002391, 2021.

994 McClure-Begley, A. Petropavlovskikh, I. and Oltmans, S.: NOAA Global Monitoring Surface Ozone
995 Network. 1973-2014. National Oceanic and Atmospheric Administration, Earth Systems Research
996 Laboratory Global Monitoring Division. Boulder, CO, doi:10.7289/V57P8WBF, 2014.

997 Mcnamara, S. M., Kolesar, K. R., Wang, S., Kirpes, R. M., May, N. W., Gunsch, M. J., Cook, R. D.,
998 Fuentes, J. D., Hornbrook, R. S., Apel, E. C., Laskin, A. and Pratt, K. A.: Observation of Road Salt
999 Aerosol Driving Inland Wintertime Atmospheric Chlorine Chemistry, ACS Cent. Sci., 6(684–694),
1000 doi:10.1021/acscentsci.9b00994, 2020.

1001 Moore, C. W., Obrist, D., Steffen, A., Staebler, R. M., Douglas, T. A., Richter, A. and Nghiem, S. V:
1002 Convective forcing of mercury and ozone in the Arctic boundary layer induced by leads in sea ice.,
1003 Nature, 506(7486), 81–4, doi:10.1038/nature12924, 2014.

1004 Nghiem, S.: Studying bromine, ozone, and mercury chemistry in the Arctic, Eos, Trans. Am. Geophys.
1005 Union, 94(33), 289–291, doi:10.1038/NGEO1779., 2013.

1006 Oltmans, S. J., Johnson, B. J. and Harris, J. M.: Springtime boundary layer ozone depletion at Barrow,
1007 Alaska: Meteorological influence, year-to-year variation, and long-term change, J. Geophys. Res. Atmos.,
1008 117(8), 1–18, doi:10.1029/2011JD016889, 2012.

1009 Oum, K. W., Lakin, M. J. and Finlayson-Pitts, B. J.: Bromine activation in the troposphere by the dark
1010 reaction of O 3 with seawater ice, Geophys. Res. Lett., 25(21), 3923–3926, doi:10.1029/1998GL900078,
1011 1998.

1012 Parrella, J. P., Jacob, D. J., Liang, Q., Zhang, Y., Mickley, L. J., Miller, B., Evans, M. J., Yang, X., Pyle,
1013 J. A., Theys, N. and Van Roozendael, M.: Tropospheric bromine chemistry: Implications for present and
1014 pre-industrial ozone and mercury, Atmos. Chem. Phys., 12(15), 6723–6740, doi:10.5194/acp-12-6723-
1015 2012, 2012.

1016 Payne, V. H., Clough, S. A., Shephard, M. W., Nassar, R. and Logan, J. A.: Information-centered
1017 representation of retrievals with limited degrees of freedom for signal : Application to methane from the
1018 Tropospheric Emission Spectrometer, J. Geophys. Res., 114, 1–16, doi:10.1029/2008JD010155, 2009.

1019 Peterson, P. K., Simpson, W. R., Pratt, K. A., Shepson, P. B., Frieß, U., Zielcke, J., Platt, U., Walsh, S. J.
1020 and Nghiem, S. V.: Dependence of the vertical distribution of bromine monoxide in the lower troposphere
1021 on meteorological factors such as wind speed and stability, Atmos. Chem. Phys., 15, 2119–2137,
1022 doi:10.5194/acp-15-2119-2015, 2015.

1023 Peterson, P. K., Pöhler, D., Sihler, H., Zielcke, J., General, S., Frieß, U., Platt, U., Simpson, W. R.,
1024 Nghiem, S. V., Shepson, P. B., Stirm, B. H., Dhaniyala, S., Wagner, T., Caulton, D. R., Fuentes, J. D. and
1025 Pratt, K. A.: Observations of bromine monoxide transport in the Arctic sustained on aerosol particles,
1026 Atmos. Chem. Phys., 17(12), 7567–7579, doi:10.5194/acp-17-7567-2017, 2017.

1027 Peterson, P. K., Pöhler, D., Zielcke, J., General, S., Friess, U., Platt, U., Simpson, W. R., Nghiem, S.,
1028 Shepson, P. B., Stirm, B. H. and Pratt, K. A.: Springtime Bromine Activation Over Coastal and Inland
1029 Arctic Snowpacks, ACS Earth Sp. Chem., acsearthspacechem.8b00083,
1030 doi:10.1021/acsearthspacechem.8b00083, 2018.

1031 Peterson, P. K., Hartwig, M., May, N. W., Schwartz, E., Rigor, I., Ermold, W., Steele, M., Morison, J. H.,
1032 Nghiem, S. V and Pratt, K. A.: Snowpack measurements suggest role for multi-year sea ice regions in
1033 Arctic atmospheric bromine and chlorine chemistry, Elementa, 2019.

1034 Pöhler, D., Vogel, L., Friess, U. and Platt, U.: Observation of halogen species in the Amundsen Gulf,
1035 Arctic, by active long-path differential optical absorption spectroscopy., Proc. Natl. Acad. Sci. U. S. A.,
1036 107(15), 6582–7, doi:10.1073/pnas.0912231107, 2010.

1037 Pound, R. J., Sherwen, T., Helmig, D., Carpenter, L. J. and Evans, M. J.: Influences of oceanic ozone
1038 deposition on tropospheric photochemistry, Atmos. Chem. Phys., 20(7), 4227–4239, doi:10.5194/acp-20-
1039 4227-2020, 2020.

1040 Pratt, K. A., Custard, K. D., Shepson, P. B., Douglas, T. A., Pöhler, D., General, S., Zielcke, J., Simpson,
1041 W. R., Platt, U., Tanner, D. J., Gregory Huey, L., Carlsen, M. and Stirm, B. H.: Photochemical production
1042 of molecular bromine in Arctic surface snowpacks, Nat. Geosci., 6(5), 351–356, doi:10.1038/ngeo1779,
1043 2013.

1044 Richter, A., Wittrock, F., Eisinger, M. and Burrows, J. P.: GOME observations of tropospheric BrO in
1045 Northern Hemispheric spring and summer 1997, Geophys. Res. Lett., 25(14), 2683–2686,
1046 doi:10.1029/98GL52016, 1998.

1047 Rodgers, C. D. and Connor, B. J.: Intercomparison of remote sounding instruments, J. Geophys. Res.,
1048 108(March 2002), doi:10.1029/2002JD002299, 2003.

1049 Saiz-Lopez, A. and von Glasow, R.: Reactive halogen chemistry in the troposphere, Chem. Soc. Rev.,
1050 41(19), 6448, doi:10.1039/c2cs35208g, 2012.

1051 Salawitch, R. J., Canty, T., Kurosu, T., Chance, K., Liang, Q., Silva, A., Pawson, S., Nielsen, J. E.,
1052 Rodriguez, J. M., Bhartia, P. K., Liu, X., Huey, L. G., Liao, J., Stickel, R. E., Tanner, D. J., Dibb, J. E.,
1053 Simpson, W. R., Donohoue, D., Kreher, K., Johnston, P. V, Gao, R. S., Johnson, B., Bui, T. P. and Chen,
1054 G.: A new interpretation of total column BrO during Arctic spring, Geophys. Res. Lett., 37(21), 1–9,
1055 doi:10.1029/2010GL043798, 2010.

1056 Sander, R., Keene, W. C., Pszenny, A. A. P., Arimoto, R., Ayers, G. P., Baboukas, E., Cainey, J. M.,
1057 Crutzen, P. J., Duce, R. A., Hönninger, G., Huebert, B. J., Maenhaut, W., Mihalopoulos, N., Turekian, V.
1058 C. and Van Dingenen, R.: Inorganic bromine in the marine boundary layer: A critical review, Atmos.
1059 Chem. Phys., 3(5), 1301–1336, doi:10.5194/acp-3-1301-2003, 2003.

1060 Schmidt, J. A., Jacob, D. J., Horowitz, H. M., Hu, L., Sherwen, T., Evans, M. J., Liang, Q., Suleiman, R.
1061 M., Oram, D. E., Le Breton, M., Percival, C. J., Wang, S., Dix, B. and Volkamer, R.: Modeling the
1062 observed tropospheric BrO background: Importance of multiphase chemistry and implications for ozone,
1063 OH, andmercury, J. Geophys. Res., 121(19), 11819–11835, doi:10.1002/2015JD024229, 2016.

1064 Schroeder, W. H., Anlauf, K. G., Barrie, L. A., Lu, J. Y. and Steffen, A.: Arctic Springtime Depletion of
1065 Mercury, Nature, 394, 331–332, doi:10.1038/379126b0, 1998.

1066 Shah, V., Jacob, D. J., Moch, J. M., Wang, X. and Zhai, S.: Global modeling of cloud water acidity ,
1067 precipitation acidity , and acid inputs to ecosystems, Atmos. Chem. Phys, 12223–12245, 2020.

1068 Sherwen, T., Schmidt, J. A., Evans, M. J., Carpenter, L. J., Großmann4, K., Eastham, S. D., J., D. J., Dix,
1069 B., Koenig, T. K., Sinreich, R., Ortega, I., Volkamer, R., Saiz-Lopez, A., Prados-Roman, C., Mahajan, A.
1070 S. and C. Ordóñez: DISCUSS Global impacts of tropospheric halogens (Cl, Br, I) on oxidants and
1071 composition in GEOS-Chem, Atmos. Chem. Phys. Discuss., (May), doi:10.5194/acp-2016-424, 2016a.

1072 Sherwen, T., Schmidt, J. A., Evans, M. J., Carpenter, L. J., Großmann, K., Eastham, S. D., Jacob, D. J.,
1073 Dix, B., Koenig, T. K., Sinreich, R., Ortega, I., Volkamer, R., Saiz-Lopez, A., Prados-Roman, C.,
1074 Mahajan, A. S. and Ordóñez, C.: Global impacts of tropospheric halogens (Cl, Br, I) on oxidants and
1075 composition in GEOS-Chem, Atmos. Chem. Phys., 16(18), 12239–12271, doi:10.5194/acp-16-12239-
1076 2016, 2016b.

1077 Sherwen, T., Evans, M. J., Carpenter, L. J., Schmidt, J. A. and Mickely, L. J.: Halogen chemistry reduces
1078 tropospheric O3 radiative forcing, Atmos. Chem. Phys., (August), 1–18, doi:10.5194/acp-2016-688,
1079 2016c.

1080   Simpson, W. R.: Atmospheric measurements via Multiple Axis Differential Optical Absorption
1081   Spectroscopy (MAXDOAS), Utqiagvik (Barrow), Alaska 2012-2018. Arctic Data Center, Arcticdata.io,
1082   doi:10.18739/A2222R550, 2018.

1083   Simpson, W. R., Perovich, D. K., Matrai, P. A., Shepson, P. B. and Chavez, F.: The Collaborative O-
1084   Buoy Project: Deployment of a Network of Arctic Ocean Chemical Sensors for the IPY and beyond.
1085   Arctic Data Center, doi:10.18739/A2WD4W, 2009.

1086   Simpson, W. R., Brown, S. S., Saiz-Lopez, A., Thornton, J. A. and Glasow, R. Von: Tropospheric
1087   Halogen Chemistry: Sources, Cycling, and Impacts, Chem. Rev., 150312153236002,
1088   doi:10.1021/cr5006638, 2015.

1089   Simpson, W. R., Peterson, P. K., Frieß, U., Sihler, H., Lampel, J., Platt, U., Moore, C., Pratt, K., Shepson,
1090   P., Halfacre, J. and Nghiem, S. V: Horizontal and vertical structure of reactive bromine events probed by
1091   bromine monoxide MAX-DOAS, Atmos. Chem. Phys., 17, 9291–9309, 2017.

1092   Stutz, J., Thomas, J. L., Hurlock, S. C., Schneider, M., Von Glasow, R., Piot, M., Gorham, K., Burkhart,
1093   J. F., Ziemba, L., Dibb, J. E. and Lefer, B. L.: Longpath DOAS observations of surface BrO at Summit,
1094   Greenland, Atmos. Chem. Phys., 11(18), 9899–9910, doi:10.5194/acp-11-9899-2011, 2011.

1095   Swanson, W. F., Graham, K. A., Halfacre, J. W., Holmes, C. D., Shepson, P. B. and Simpson, W. R.:
1096   Arctic Reactive Bromine Events Occur in Two Distinct Sets of Environmental Conditions : A Statistical
1097   Analysis of 6 Years of Observations Journal of Geophysical Research : Atmospheres, 1–19,
1098   doi:10.1029/2019JD032139, 2020.

1099   Tang, T. and McConnell, J. C.: Autocatalytic release of bromine from Arctic snow pack during polar
1100   sunrise, Geophys. Res. Lett., 23(19), 2633–2636, doi:10.1029/96GL02572, 1996.

1101   Theys, N., Van Roozendael, M., Hendrick, F., Yang, X., De Smedt, I., Richter, A., Begoin, M., Errera,
1102   Q., Johnston, P. V., Kreher, K. and De Maziere, M.: Global observations of tropospheric BrO columns
1103   using GOME-2 satellite data, Atmos. Chem. Phys., 11(4), 1791–1811, doi:10.5194/acp-11-1791-2011,
1104   2011.

1105   Thomas, J. L., Stutz, J., Lefer, B., Huey, L. G., Toyota, K., Dibb, J. E. and Von Glasow, R.: Modeling
1106   chemistry in and above snow at Summit, Greenland - Part 1: Model description and results, Atmos.
1107   Chem. Phys., 11(10), 4899–4914, doi:10.5194/acp-11-4899-2011, 2011.

1108   Toom-Sauntry, D. and Barrie, L. A.: Chemical composition of snowfall in the high Arctic: 1990-1994,
1109   Atmos. Environ., 36(15–16), 2683–2693, doi:10.1016/S1352-2310(02)00115-2, 2002.

1110   Toyota, K., McConnell, J. C., Lupu, A., Neary, L., McLinden, C. A., Richter, A., Kwok, R., Semeniuk,
1111   K., Kaminski, J. W., Gong, S.-L., Jarosz, J., Chipperfield, M. P. and Sioris, C. E.: Analysis of reactive
1112   bromine production and ozone depletion in the Arctic boundary layer using 3-D simulations with GEM-
1113   AQ: inference from synoptic-scale patterns, Atmos. Chem. Phys., 11(8), 3949–3979, doi:10.5194/acp-11-
1114   3949-2011, 2011.

1115   Toyota, K., Mcconnell, J. C., Staebler, R. M. and Dastoor, A. P.: Air – snowpack exchange of bromine ,
1116   ozone and mercury in the springtime Arctic simulated by the 1-D model PHANTAS – Part 1 : In-snow
1117   bromine activation and its impact on ozone, Atmos. Chem. Phys., 4101–4133, doi:10.5194/acp-14-4101-
1118   2014, 2014.

1119   Travis, K. R., Jacob, D. J., Fisher, J. A., Kim, P. S., Marais, E. A., Zhu, L., Yu, K., Miller, C. C.,
1120   Yantosca, R. M., Sulprizio, M. P., Thompson, A. M., Wennberg, P. O., Crounse, J. D., St Clair, J. M.,
1121   Cohen, R. C., Laughner, J. L., Dibb, J. E., Hall, S. R., Ullmann, K., Wolfe, G. M., Pollack, I. B., Peischl,
1122   J., Neuman, J. A. and Zhou, X.: Why do models overestimate surface ozone in the Southeast United

1123   States?, Atmos. Chem. Phys., 16(21), 13561–13577, doi:10.5194/acp-16-13561-2016, 2016.

1124   Vogt, R., Crutzen, P. and Sander, R.: A mechanism for halogen release from sea-salt, Nature,
1125   383(September), 327–331, 1996.

1126   Wagenbach, D., Minikin, A., Ducroz, F., Mulvaney, R., Keck, L., Legrand, M., Hall, J. S. and Wolff, E.
1127   W.: Sea-salt aerosol in coastal Antarctic regions at three coastal, J. Geophys. Res. Atmos., 103, 961–974,
1128   1998.

1129   Wagner, T. and Platt, U.: Satellite mapping of enhanced BrO concentrations in the troposphere, Nature,
1130   395(October), 486–490, doi:10.1038/26723, 1998.

1131   Wang, S. and Pratt, K. A.: Molecular Halogens Above the Arctic Snowpack: Emissions, Diurnal
1132   Variations, and Recycling Mechanisms, J. Geophys. Res. Atmos., 122(21), 11,991-12,007,
1133   doi:10.1002/2017JD027175, 2017.

1134   Wang, S., Mcnamara, S. M., Moore, C. W., Obrist, D., Steffen, A., Shepson, P. B., Staebler, R. M., Raso,
1135   A. R. W. and Pratt, K. A.: Direct detection of atmospheric atomic bromine leading to mercury and ozone
1136   depletion, Proc. Natl. Acad. Sci., 116(29), doi:10.18739/A2D79598P.1, 2019a.

1137   Wang, X., Jacob, D. J., Eastham, S. D., Sulprizio, M. P., Zhu, L., Chen, Q., Alexander, B., Sherwen, T.,
1138   Evans, M. J., Lee, B. H., Haskins, J. D., Lopez-hilfiker, F. D., Thornton, J. A., Huey, G. L. and Liao, H.:
1139   The role of chlorine in global tropospheric chemistry, Atmos. Chem. Phys, 3981–4003, 2019b.

1140   Wang, X., Jacob, D. J., Downs, W., Zhai, S., Zhu, L., Shah, V., Holmes, C. D., Sherwen, T., Alexander,
1141   B., Evans, M. J., Eastham, S. D., Neuman, J. A., Veres, P. R., Koenig, T. K., Volkamer, R., Huey, L. G.,
1142   Bannan, T. J., Percival, C. J., Lee, B. H. and Thornton, J. A.: Global tropospheric halogen (Cl, Br, I)
1143   chemistry and its impact on oxidants, Atmos. Chem. Phys., 21(18), 13973–13996, doi:10.5194/acp-21-
1144   13973-2021, 2021.

1145   Wennberg, P. O.: Bromine explosion, Nature, 397(6717), 299–301, doi:10.1038/16805, 1999.

1146   Wren, S. N., Kahan, T. F., Jumaa, K. B. and Donaldson, D. J.: Spectroscopic studies of the heterogeneous
1147   reaction between O 3(g) and halides at the surface of frozen salt solutions, J. Geophys. Res. Atmos.,
1148   115(16), 1–8, doi:10.1029/2010JD013929, 2010.

1149   Wren, S. N., Donaldson, D. J. and Abbatt, J. P. D.: Photochemical chlorine and bromine activation from
1150   artificial saline snow, Atmos. Chem. Phys., 13(19), 9789–9800, doi:10.5194/acp-13-9789-2013, 2013.

1151   Yang, X., Pyle, J. A. and Cox, R. A.: Sea salt aerosol production and bromine release: Role of snow on
1152   sea ice, Geophys. Res. Lett., 35(16), 1–5, doi:10.1029/2008GL034536, 2008.

1153   Yang, X., Pyle, J. A., Cox, R. A., Theys, N. and Van Roozendael, M.: Snow-sourced bromine and its
1154   implications for polar tropospheric ozone, Atmos. Chem. Phys., 10(16), 7763–7773, doi:10.5194/acp-10-
1155   7763-2010, 2010.

1156   Yang, X., Frey, M., Rhodes, R., Norris, S., Brooks, I., Anderson, P., Nishimura, K., JOnes, A. and Wolff,
1157   E.: Sea salt aerosol production via sublimating wind-blown saline snow particles over sea ice:
1158   parameterizations and relevant microphysical mechanisms, Atmos. Chem. Phys., 19, 8407–8424, 2019.

1159   Zhu, L., Jacob, D. J., Eastham, S. D., Sulprizio, M. P., Wang, X., Sherwen, T., Evans, J., Chen, Q.,
1160   Alexander, B., Koenig, T. K., Volkamer, R. and Huey, L. G.: Effect of sea salt aerosol on tropospheric
1161   bromine chemistry, Atmos. Chem. Phys., 6497–6507, 2019.

1162